THESIS

MODELING OF TWISTED AND COILED ARTIFICIAL MUSCLE FOR ACTUATION AND SELF-SENSING

Submitted by

Ali Abbas

Department of Mechanical Engineering

In partial fulfillment of the requirements

For the Degree of Master of Science

Colorado State University

Fort Collins, Colorado

Spring 2018

Master's Committee:

Advisor: Jianguo Zhao

Thomas Bradley
Anthony Maciejewski

ABSTRACT

MODELING OF TWISTED AND COILED ARTIFICIAL MUSCLE FOR ACTUATION AND SELF-SENSING

Soft robots are a new type of robots with deformable bodies and muscle-like actuations, which are fundamentally different from traditional robots with rigid links and motor-based actuators. Owing to their elasticity, soft robots outperform rigid ones in safety, maneuverability, and adaptability. With their advantages, many soft robots have been developed for manipulation and locomotion in recent years. Nevertheless, two issues prevent the wide applications of developed soft robots: cumbersome actuation methods (e.g., pneumatics) and limited sensing capability to feedback the robot's shape. To address these two issues, this thesis leverages a recently discovered twisted and coiled artificial muscle for soft robots. This artificial muscle can generate large force and displacement; moreover, we recently found that it has self-sensing capability, i.e., its electrical resistance will increase if the muscle is elongated by an external force. With the dual actuation and self-sensing capability, we expect to accomplish closed-loop control of soft robots for precise motion without external sensors, potentially solving the two issues for existing soft robots.

This thesis will focus on three aspects for the twisted and coiled artificial muscle. First, we model the actuation from a physics perspective. Such a model utilizes parameters related to the working principle and material properties of the actuator, eliminating the requirements for tedious system identifications. Experiments are conducted to verify the proposed model, and the results demonstrate that the proposed model can predict the static performance and dynamic response for the muscle. Second, we test and model the sensing capability of the artificial muscle. Specifically, we establish a physics-based model to predict the external force and the displacement if the resistance is given and experimentally validate its correctness. Third, we apply the actuation and sensing of the artificial muscle to soft robots. To demonstrate we can leverage the muscle to actuate

soft robots, we fabricate a soft manipulator with multiple muscles as well as a robotic fish tail. To demonstrate the sensing capability, we embed the muscle into soft materials and successfully measure two curvatures of a two-segment soft robot. Based on the work presented in this thesis, our future work will integrate the actuation and sensing capability of the twisted and coiled artificial muscle to enable closed-loop shape control of soft robots.

ACKNOWLEDGEMENTS

I would like thank my advisor Dr. Jianguo Zhao from the core of my heart for providing me with the opportunity to work on this project. He has guided me and supervised me in best possible way. It is through his patience and vision that I have been able to achieve substantially as a student researcher. I am thankful to Dr. Thomas Bradley and Dr. Anthony Maciejewski for accepting to review and evaluate this thesis as my committee member and making the thesis defense possible. I would also like to thank my colleagues and friends who have always been very supportive and have believed in my abilities.

Finally, I would like to thank my parents and siblings who have been with me through thick and thin. I am grateful for their confidence and belief in me. It is the fruit of their prayers and wishes that I have been able to come up with this thesis.

DEDICATION

I would like to dedicate this thesis to my family, teachers and friends.

TABLE OF CONTENTS

LIST OF FIGURES

Chapter 1

Introduction

1.1 Soft Robots Vs Traditional Robots

Soft robots have bodies made from inherently soft and flexible materials such as silicone, silicone rubber etc. On the contrary, conventional robots have rigid bodies with metallic links and joints which may have sharp edges. Hence, their interaction with humans can be unsafe. Whereas, soft robots owing to their inherently soft structure can deform and absorb much of the impact caused by a collision. Therefore, the soft robots provide an opportunity to bridge the gap between machines and people. The conventional robots with rigid bodies are used extensively in manufacturing and can be specifically programmed to perform a single task effectively but often their adaptability is limited. Whereas, soft robots with compliant bodies are of importance in the systems that deal with uncertain and dynamic environments. Their soft body allows them to handle products of different shapes and sizes. They can pick up an object as delicate as an egg without crushing it. These robots have a continuously deformable structure which results in a relatively large number of degrees of freedom compared with their hard-bodied counterparts.

Conventional robots, made from motors and metal bearings, are great for tasks such as spot-welding and painting cars. Whereas, soft robots have the potential to exhibit unprecedented adaptation, sensitivity and agility. A traditional rigid-bodied robot and a soft robot is shown in Figure1.1a and Figure1.1b respectively. We will summarize three major differences between these two types of robots. One, the traditional robots have rigid links made from metals and their alloys. This rigidity of the traditional robots limits their adaptability to new tasks and environments. Whereas, soft robots have flexible parts and limbs made from soft materials like plastic, silicone etc. making them compliant to dynamic environments. Second, traditional robots have fixed degree of freedom, while soft robots have infinite degrees of freedom. Third, because of the order of DOF the shape estimation is much more difficult in soft robots than in traditional robots.

Soft robots can be used in confined spaces because of their potential to be able to bend and twist with high number of curvatures [2]. Marchese *et al.* has demonstrated a soft robotic manipulation system that is capable of autonomous, dynamic, and safe interactions with humans and its environment [3]. Tolley *et al.* has shown that soft robots are resilient to harsh conditions such as large external forces and extreme temperatures [4]. They can deform their bodies in a continuous manner and thus emulate biological motions [5]. Soft robots can also perform rapid and agile maneuvers, such as the escape maneuver of a fish [6]. They adapt the shape of the environment, employing compliant motion and thus manipulating objects [7].

1.2 Major Challenges Faced by Soft Robots

Because of their advantages many soft robots have been developed recently. However, there are two major challenges faced by soft robots which curtails the wide applications of novel soft robotic systems. First, existing actuation methods cannot enable untethered soft robots, which are important for untethered locomotion. The actuators used are bulky and inefficient which complicates the robot design and the output is not sufficient. Second, the sensing mechanisms are not capable enough to effectively provide the real-time shape estimation of robot. The sensors that are used are either limited to certain environments or not capable of providing with shape estimation of continuously deforming multi-curvature soft robot.

Despite the differences between rigid and soft robots, the actuators that are mostly used in soft robots are similar to the actuators used in rigid-bodied robots. These actuators have bulky parts like valves, hydraulic and pneumatic pumps etc., making the robot design and fabrication a complex job. A different actuator is still needed for soft robots, one that is simple in design and easy to fabricate. One that can be embedded inside a soft robot and can generate actuation from within the body of the robot. Therefore, in this thesis we will present a soft artificial muscle actuator. This actuator is much simpler in design and do not have large bulky parts, hence it can be embedded inside a soft robot. An artificial muscle actuator is a type of actuator that can mimic the motion of a biological muscle. It is an actuator that can reversibly contract, expand

and rotate within the body on the application of an external stimuli [8] (e.g. voltage, heat etc.). Artificial muscles can be divided into three major groups which are based on the type of stimulus that actuates them. i) Electric field actuation, ii) Ion-based actuation and iii) Thermal actuation. Some of these artificial muscles are named here: Dielectric Elastomer Actuators (DEA) [9], Ionic Polymer-Metal Composites (IPMC) [10, 11] and Shape Memory Alloys (SMA) [12]. However, these actuators do not show better performance than their biological counterpart. Whereas, the Twisted and Coiled Artificial Muscle (TCAM) constructed from ordinary fishing line and sewing thread can lift more weight and generate more power than a biological muscle of the same length and weight [13].

Another important aspect of the soft robotics is to sense the shape of the soft robot during and/or after actuation, which can allow us to control the robot motion precisely. Since soft robots have a continuously deforming shape and infinite degrees of freedom, the sensing approach used in soft robots is different from the one used in traditional robots. In traditional robots, one approach is to place a simple encoder at the joint of the robot which can record the change in angle when the joint is actuated. Based on this angle the location of the end-effector can be easily determined. Whereas, sensors in soft robots can be divided into two types, internal sensors and external sensors. An internal sensor can be embedded inside the soft body of the robot and can provide with the shape estimation of the robot when it deforms. Examples of internal sensors are optical fibers used in continuum robots [14] and soft robots [15, 16], liquid metal [17, 18], miniature magnets and hall-effect sensors [19]. However, a major limitation of the internal sensor is that it can only measure single curvature of the soft robot, but a soft robot deforms continuously and can have multiple curvatures. The external sensors use cameras to capture the images of the actuating robot. These images are then processed to estimate the curvature of the robot [3, 20]. Electromagnetic sensors are also used to reconstruct the shape of soft robots [21]. The limitation with such external sensors is that they are large, require line of sight for cameras and non-magnetic environments for electromagnetic sensors.

1.3 TCAM as Actuator and Sensor

TCAMs are actuators that can tremendously mimic the motion of a biological muscle. In fact, in a recent breakthrough researchers have reported a TCAM actuator that can surpass the performance of its biological counterpart [13]. These TCAMs can actuate longitudinally when heated. Polymer fibers like monofilament nylon fishing line and conductive sewing threads are used to fabricate them. Based on the fabrication process a TCAM actuator is referred to as Twisted and Coiled Actuator (TCA) since it is first twisted and then coiled to achieve its final shape. There are many advantages of TCA. For example they are very low cost and easy to fabricate, they are highly customizable, based on the fabrication process a TCA can be made to either contract or elongate and the most important advantage is that they have shown better performance than existing artificial muscle actuators and biological muscles [13]. These advantages have allowed the TCAs to be used in a number of applications, e.g., robotic arm [22], actuating textile [13] etc.

Even though there are many applications of TCA, the theoretical models that have been developed to predict the actuation response of TCA are scarce. The prediction of actuation response provides with the bases for precise motion control of soft robots. Few of the developed models are listed here: A dynamic model for TCA has been established by Yip *et al.* [22] . Another dynamic model has been demonstrated by Arakawa *et al.* [23], with a focus on position control, but these models are not from physics perspective and require experimentally identified parameters. A multiscale approach has been adopted by Yang *et al.* [24], but this multiscale approach involves a large number of parameters which makes fast computation required for feedback control complex. Even though, a physics based model has been demonstrated by Haines *et al.* [13], but experimental setups have been used to measure important parameters required in the model. Therefore, a simple but accurate model feasible for real time control is still required, one that is based on physical parameters of the TCA and does not require any experimentation to identify these parameters.

As recently discovered by Zhao *et al.* [25] and Joost *et al.* [26], TCAMs also have the ability to work as a sensor when embedded inside a soft robot. From the recent work on TCAM, it can be inferred that researchers have mainly focused on theoretical modeling and their applications as

Figure 1.1: (a) Traditional rigid-bodied robot. (b) Soft robot. (Picture taken from [1]).

actuators. The TCAM used as a sensor will be referred to as Twisted and Coiled Sensor (TCS). Experiments have shown [25] that the electrical resistance of the TCS changes with the change in its length. In this thesis, we have investigated this new TCS that can be used to relate the change of its resistance with the change in its length, providing the bases of shape estimation of multiple curvatures of soft robot, which outperforms the existing internal sensors that can only estimate a single curvature. A sensing model based on physical parameters that addresses this limitation and harness the sensing capability of TCS has also been developed. This model can use the resistance change to estimate the shape change of multi-curvature soft robots.

There are three main contributions of this thesis: i). Harness the actuation of TCAMs and develop a physics based model that can predict actuation response of TCA precisely. Whereas, current modeling approaches are not physics based and involve a number of parameters to simulate the models. The actuation model that we have developed can predict both the static and dynamic response of the TCA very precisely. ii). Develop a sensing model that can harness the self-sensing capability of the TCS and can estimate the shape change of a multi-curvature soft robot. The accuracy of the sensing model has been tested and validated by comparing the modeling results with the experimental results. iii). Demonstrate the robotic applications of TCAM both as an actuator and as a sensor.

The rest of the thesis is organized as follows: Chapter 2, discusses about the development of static and dynamic model for capturing the static and dynamic response of the TCA. It also details the accuracy of the models by comparing the modeling results with the experimental results. Chapter 3, describes the self-sensing aspect of the TCAM. It details how a TCAM can be leveraged to be used as a sensor that can precisely predict the multi-curvature configuration of a soft robot in which the TCS has been embedded. In Chapter 4, we have demonstrated the robotic applications of both the TCA and TCS and in Chapter 5, we have drawn conclusions of our work and also discussed the future work.

Chapter 2

A Physics-Based Model for Twisted and Coiled Actuator

2.1 Introduction

Artificial muscles, unlike traditional electric motors, can generate life-like motions similar to biological muscles. Many artificial muscles have been investigated in order to achieve similar capabilities of their biological counterparts, and we briefly review several representative ones here. Shape Memory Alloys (SMA), a combination of different metals, can generate linear displacements through thermal induced phase changes [12]. Ionic Polymer-Metal Composites (IPMC), by sandwiching a polymer layer between two metal electrodes, can generate bending motion if a voltage is applied due to the ion migration [10, 11]. Dielectric Elastomer Actuators (DEA), composed of an elastomer membrane sandwiched between two compliant electrodes, can expand in surface area owing to forces generated by opposite charges on electrodes [9]. However, all of existing artificial muscles can only generate either limited forces or limited displacements, making them inferior to biological muscles.

Recently, Haines *et al.* discovered a new artificial muscle that was made from ordinary polymer fibers such as fishing line or sewing thread [13]. The muscle can be conveniently fabricated by first twisting a polymer fiber and then coiling the twisted fiber into a helical spring-like structure. The fabrication process of the twisted and coiled actuator (TCA) is detailed in the next section. The resulting TCA can contract or extend if heated due to thermal expansion of twisted fiber [13]. In fact, if temperature increases, the twisted fiber will contract in axial direction and expand in radial direction, both of which will lead to an untwisting torque, resulting in the linear actuation of TCA.

There are three advantages for TCA compared with existing artificial muscles. First, it is low cost because of the widely available inexpensive fishing line or sewing thread. For example, the

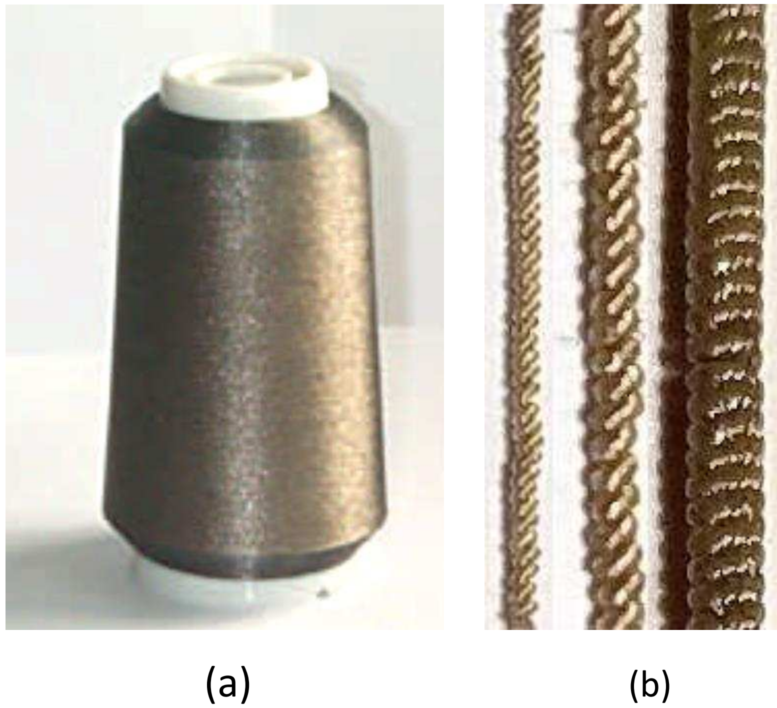

Figure 2.1: Twisted and coiled actuator (TCA) can be fabricated from sewing threads. (a) A cone of conductive sewing thread. (b) Fabricated TCAs with different diameters: 0.36mm, 0.76mm, 1.3mm.

conductive sewing threads shown in Figure. 2.1a can be purchased for $\$0.3$ per meter. Second, TCAs have better performances in terms of force and displacement. In fact, it can contract up to 49% and generate force 100 times larger than human muscle of the same weight and length [13]. Third, TCAs are highly customizable. Different TCAs with desired performance can be fabricated under specific conditions as illustrated in Figure. 2.1b. Moreover, depending on the twisting and coiling directions, the resulting TCA can extend, which is generally infeasible for existing artificial muscles.

Because of their advantages, TCAs have been employed for many robotic applications including robotic hand [22, 27], robot skin [28], robotic finger [29], deformable rolling robot [30], morphing wings for flying robot [31], assistive wrist orthosis [32], and bending muscles [33], etc.

Despite many applications, only a few works try to develop theoretical models to capture and predict the actuator's static and dynamic behaviors, which is crucial for the precise control of the actuator's motion. Yip and Niemeyer established a dynamic model for TCAs by combining a thermo-mechanical and thermo-electrical model [22, 34]. They also validated their model through closed-loop force and position control. Nevertheless, their model was from control system perspective and required to identify parameters through many experiments. Arakawa *et al* performed similar studies focusing on position control [23]. Yang and Li developed a multiscale approach to derive the thermo-mechanical actuation response of TCAs [24]. By building a series of models from nanoscale, microscale, mesoscale, to macroscale, they could predict the static performance of TCAs. However, this multiscale approach involved a large number of parameters which are generally material properties such as tensile and shear modulus, coefficient of thermal expansion, elastic constants etc, which is too complex for fast computations that is required for feedback control. Therefore, a simple but accurate model that is amiable for real time control is still needed.

In this chapter, we aim to propose a physics based model to capture the relationship between temperate, force, and displacement for TCA. This model is based on the underlying working principle: thermal expansions due to the increase of temperature for the twisted fiber. We first obtain the temperature induced torque in twisted fibers, and then relate this torque to the actuator's linear displacement through a consistent model of spring-like structure. Based on the static model, we also establish a dynamic model to capture the dynamic behavior of TCAs. Both the static and dynamic models are verified by experimental results.

The main contribution of this chapter is a new model for the newly discovered TCA and experimental validations of proposed models. Compared with the model established using system identifications [22, 34], it is from the physics perspective and can be readily applied to any TCA if the material properties are known. Compared with the multiscale approach [24], the proposed model is simpler since it only considers the macroscale motion; consequently, it will be more computational efficient, which is better for closed-loop control.

The rest of this chapter is organized as follows. In section 2.2, we discuss about the fabrication proces of the TCA. In 2.3, we detail the static model to obtain the displacement given an increase of temperature and an external force. Based on the static model, in section 2.4, we describe a dynamics model with a time-varying external force, and present the model for a specific case when the increase of temperature is generated from a voltage applied to the actuator. In section 2.5, simulation results, experimental setup and experimental results are detailed to validate the proposed models.

2.2 Fabrication of TCA

As discussed in the previous section, one of the main advantages of the TCA is the ease with which it can be fabricated. The fabrication process is comprised of three simple steps, twisting, coiling and annealing (stabilizing). These three steps are also shown in Figure 2.2. During twisting a polymer fiber (Nylon fishing line or silver coated nylon sewing thread) is attached from one of its ends to a rotating source such as DC motor, while the other end is constrained from rotation but can move horizontally and an appropriate hanging weight is also attached to it Figure 2.2a. It is important to select optimum hanging weight as it keeps the fiber stretched while twists are induced into the fiber Figure 2.2b. If the hanging weight is too small, snarling will start hence a TCA cannot be formed and if the hanging weight is too large the precursor fiber will break during twisting, hence failing the fabrication process. After a critical amount of twists are inserted to the fiber, coiling starts Figure 2.2c. The motor is kept on until the entire length of the twisted fiber is converted into coils Figure 2.2d. After acheiving the twisted and coiled configuration, the hanging weight is increased and the TCA along with the hanging weight is placed in a heating oven (shown as heating in Figure 2.2e.), which anneals the structure of the TCA and stabilizes it, so that it permanently attains this configuration and does not tend to untwist when taken out of the oven. Purpose of increasing the weight is to increase the gaps between the adjacent coils, which will provide the TCA to contract through a larger distance when actuated, hence generating a larger actuation.

2.3 Static Model

For twisted and coiled actuators (TCA), an increase of temperature will lead to the actuator's linear displacement under a constant force. However, a static model that describes the relationship

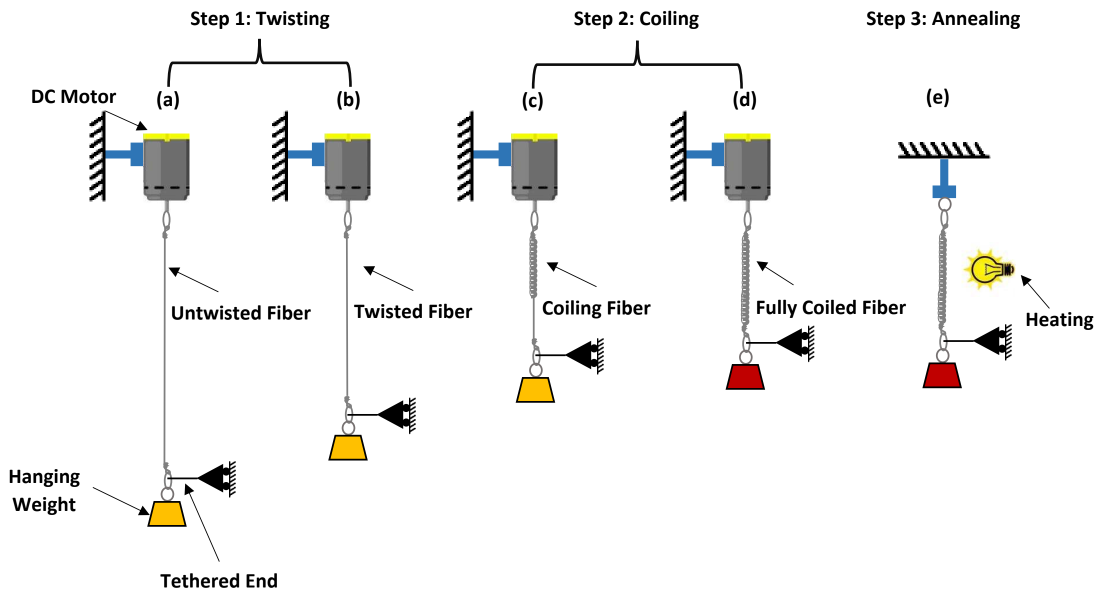

Figure 2.2: Fabrication process of a TCA. (a) Precursor polymer fiber with a hanging weight attached to it. (b) Twisted fiber made by rotating it from one end while fixing the other. (c) Initiation of the coiling. (d) Fully coiled muscle. (e) Annealing of the TCA which results in its stablilization.

between temperature, force, and displacement is not available. In this section, we will develop such a relationship from the physics perspective by combining the temperature induced torque for twisted fibers and a consistent model that relates the torque to linear displacements for helical spring-like structure. Specifically, given an actuator subject to external force F and the increase of temperature ΔT, we will solve the linear displacement δ.

2.3.1 Temperature Induced Torque for Twisted Fibers

Since the linear actuation of TCA is because of the torque generated by the twisted fiber [13], our first step is to find a relationship between an increase of temperature ΔT and the resulted torque τ.

Let ϕ_0 be the initial twist angle of a twisted fiber with length l and ϕ be the twist angle after an increase of temperature ΔT. Then $\Delta\phi = \phi_0 - \phi$ will be the untwist angle induced by the increase of temperature (refer to Figure 2.3) which suggests that the diameter of the twisted fiber increases as it tends to untwist as a result of increased temperature. Let d_0 and d be the diameter for the initial and the radially expanded twisted fiber, respectively. It is observed that the thermal

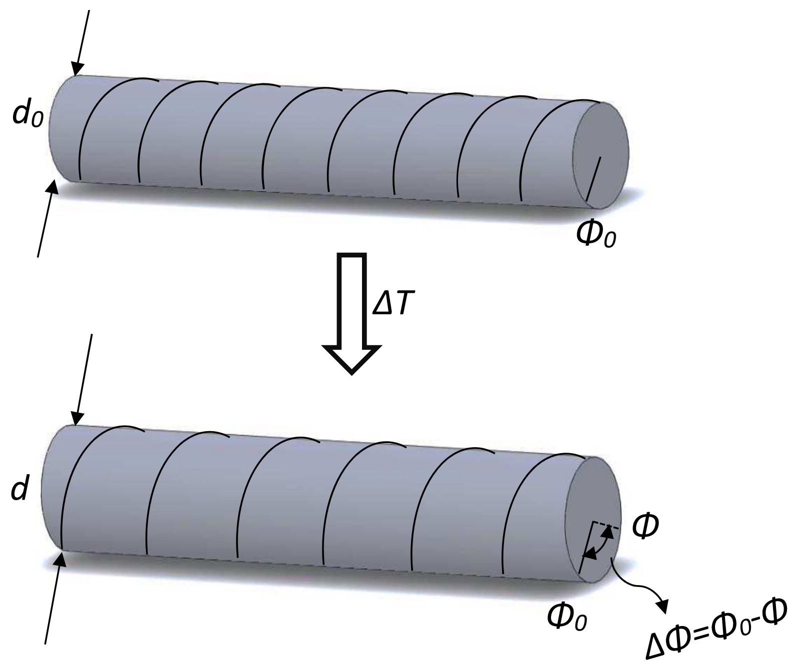

Figure 2.3: Illustration of the changing angle for twisted fibers due to an increase of temperature. The left side of the fiber is fixed, while the right side is free to rotate when temperature increases.

expansion is mainly in radial direction and the axial contraction of the fiber is almost negligible. Therefore, the ratio of the final and the intial twisted angle is equal to the ratio of the diameters [35] and is shown in (2.1).

$$\frac{\phi}{\phi_0} = \frac{d_0}{d} \tag{2.1}$$

As a result, the untwist angle can be represented by the radial expansion and initial twist angle

$$\Delta\phi = \phi_0 - \phi = \phi_0(1 - d_0/d) \tag{2.2}$$

The temperature induced torque generates shear strain γ and shear stress σ. They can be represented by standard torsion mechanics as [36]:

$$\gamma = \frac{d\Delta\phi}{2l} \tag{2.3}$$

$$\sigma = \frac{d\tau}{2J} \tag{2.4}$$

where l is the length and $J = \pi d^4/32$ is the second moment of inertia for the twisted fiber. The shear stress and strain are related through shear modulus G in the form of Hooke's law:

$$\sigma = G\gamma \tag{2.5}$$

Plugging (2.3) and (2.4) into Hooke's Law and using (2.2) gives:

$$\tau = \frac{GJ\Delta\phi}{l} = \frac{GJ\phi_0(1 - d_0/d)}{l} \tag{2.6}$$

In this equation, the only unknown is d, the diameter of the twisted fiber after temperature increase, which can be obtained using the transverse coefficient of thermal expansion ρ defined as [37]:

$$\rho = (d/d_0 - 1)/\Delta T \tag{2.7}$$

Note that ρ, a material property, can be obtained from the existing literature which provides the value for a similar material [13, 38]. With ρ, we can solve the diameter for the twisted fiber:

$$d = d_0(1 + \rho\Delta T) \tag{2.8}$$

Plugging it into (2.6), the final torque equation can be written as:

$$\tau = \frac{GJ\phi_0(1 - d_0/d)}{l} = \frac{G\phi_0\pi d_0^4(1 + \rho\Delta T)^3\Delta T\rho}{32l} \tag{2.9}$$

From this equation, the temperature induced torque can be obtained using the material properties (G and ρ), geometric parameters (l, ϕ_0, and d_0), and the increase of temperature (ΔT).

2.3.2 Linear Displacement from Temperature Induced Torque

Using the temperature induced torque, we can derive the displacement under a given external force F. In fact, the displacement δ can be obtained from the geometric relationship shown in

Figure 2.4, where α and α_0 are the current and initial pitch angle of the TCA. Assume the length of the twisted fiber l will not change since the thermal induced axial contraction is negligible, then the displacement can be obtained as:

$$\delta = l(\sin\alpha - \sin\alpha_0) \tag{2.10}$$

where α_0 is equal to the ratio between the coiled actuator length and twisted fiber length, which can be determined during the fabrication process. Whereas α which is the temperature dependent parameter is calculated by equating and solving (2.10) and (2.11) for α

On the other hand, the temperature induced torque τ and the external force F can be related through the application of Catiglianos' Second Theorem [24, 39].

$$\delta = f_{11}F - f_{12}\tau \tag{2.11}$$

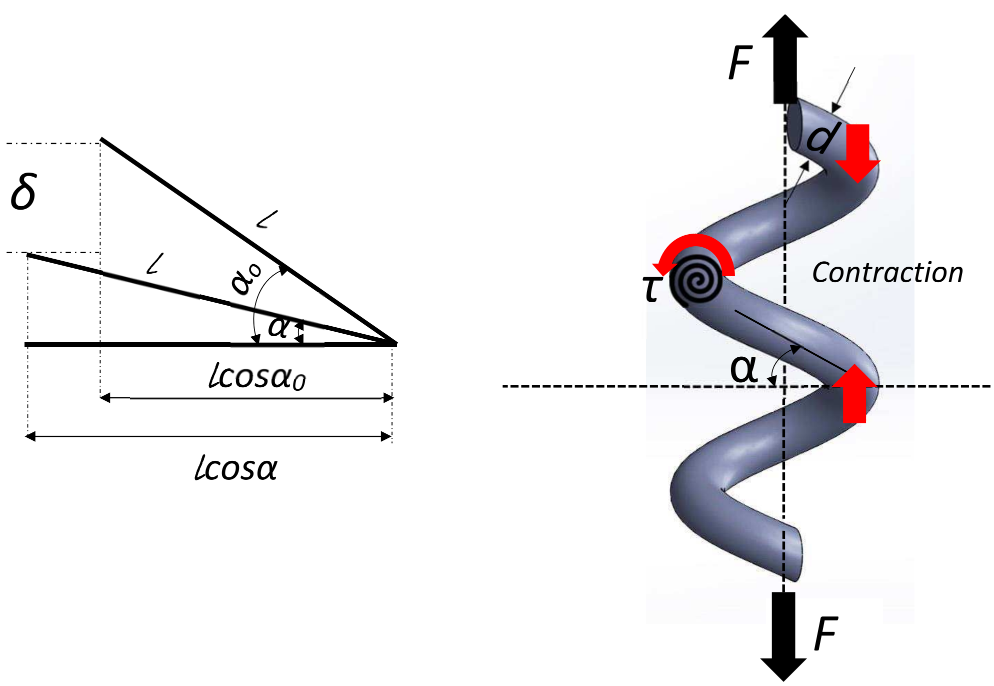

Figure 2.4: Parameters and geometric relationships for a helical spring-like structure.

where

$$
\begin{aligned}
f_{11} =& \frac{8n}{\pi^3 d^4}\left(\frac{l}{n}\right)^3 \frac{\cos^4\alpha}{G} + \frac{8n}{\pi d^2}\frac{l}{n}\frac{\cos^2\alpha}{2G} \\
&+ \frac{8n}{\pi^3 d^4}\left(\frac{l}{n}\right)^3 \frac{2\sin^2\alpha\cos^2\alpha}{E} + \frac{8n}{\pi d^2}\frac{l}{n}\frac{\sin^2\alpha}{2E} \\
f_{12} =& \frac{8n}{\pi^2 d^4}\left(\frac{l}{n}\right)^2 \frac{\cos^2\alpha}{G}
\end{aligned}
$$

In the above equation, E is the Young's Modulus of the twisted fiber, n is the number of coils of the TCA given by $n = lcos\alpha_0/(\pi D)$, where *D* is the outside diameter of the TCA [13]. The other parameters have been defined in the previous section.

Combining (2.10) and (2.11) will lead to a second order equation of $\sin^2\alpha$, which can be solved to obtain the displacement of a TCA using (2.10).

2.3.3 Direction and Temperature Dependent Modulus

Since the twisted fiber is an anisotropic polymer fiber whose mechanical properties are direction dependent [24], we employ the transverse shear modulus G_t which governs shearing in the transverse plane because the temperature induced torque given in (2.9) is a function of transverse coefficient of thermal expansion which governs the deformation in the transverse plane. Specifically, G_t can be calculated as [40]

$$G_t = \frac{4V_f E[\alpha_f/2 - \frac{1}{4}\sin(2\alpha_f)]^2}{\pi(2+\pi)(\frac{2}{3} - cos\alpha_f + \frac{1}{3}cos^3\alpha_f)(1 - cos\alpha_f)} \tag{2.12}$$

where V_f is the volume fraction of the fiber, and α_f is the fiber bias angle given as $\alpha_f = tan^{-1}(\pi d\phi)$ [13].

The elastic properties of anisotropic materials are also temperature dependent [35, 41]. For the nylon material we will use for experiment, the higher the temperature, the smaller the shear modulus. Using the data obtained in [35], we estimate that the value of the shear modulus decreases by 0.00111 GPa per Celsius degree assuming the drop is linear. As a result, the shear modulus in the torque equation should be modified as

$$G'_t = G_t - 0.00111 \times 10^6 \Delta T \tag{2.13}$$

Note that the Young's Modulus will also change with respect to temperature. However, we are not able to find relevant literature describing such a change. Therefore, we assume a constant value for E and leave a precise model for it as future work.

2.4 Dynamic Model

Let the length of a TCA be $x(t)$ with an initial length of x_0. The dynamics model for TCA should include three parts: the internal force generated in the actuator F_i due to the increase of temperature, the dynamic external force F_e, and the damping force F_d due to the velocity ($\dot{x}$) of spring-like structures. Therefore, we have

$$F_i + F_e + F_d = 0 \tag{2.14}$$

Note that the dynamics model developed in [22, 34] utilized a spring constant to obtain a force due to the displacement $\delta = x - x_0$ and a thermal constant to derive another force due to the increase of temperature $\Delta T = T - T_0$. However, these two components are included in our statics model since the internal force depends on both δ and ΔT.

The internal force F_i can be obtained using the statics model. In fact, with the statics model, we can obtain the displacement δ given the fixed external force F and temperature T. Since the external force F is balanced by the internal force generated in TCA due to δ and ΔT, we can also use the model to obtain the internal force in TCA if we know δ and ΔT. The force F in (2.11) is the external force which has a fixed value, since it is simply a hanging weight also shown in Figure 2.6. Whereas force F_i in (2.14) and (2.15) is the internal force generated by the actuator itself when the temperature of the actuator is increased. We can use the static model to calculate

F_i. If we know the displacement δ and temperature change δT we can plug these values in (2.11) and the force obtianed will be internal force F_i. It should be noted that the internal force F_i has to to overcome the external force *F* to generate certain amount of actuation δ for a given change in temperature. Hence provided the displacement and the temperature change we can account for the internal force that our actuator will generate at these inputs.

$$F_i = \frac{\delta + f_{12}\tau}{f_{11}} = \frac{x - x_0 + f_{12}\tau}{f_{11}} \tag{2.15}$$

where f_{11} and f_{12} can be solved from δ, and τ can be solved from ΔT.

The external force, depending on different situations, can be time-varying. A typical example would be a mass vertically attached to the end of the TCA. In this case,

$$F_e = m\ddot{x} - mg \tag{2.16}$$

if the coordinate is established upward.

The damping force is simply

$$F_d = b\dot{x} \tag{2.17}$$

where b is the damping coefficient, which can be obtained experimentally [22].

Given the specific profile of temperature with respect to time $T(t)$, and the initial conditions T_0 and x_0, the dynamics equation (2.14) with specific forms in (2.15), (2.16), and (2.17) can be solved to predict the dynamic response of TCA (the thermo-mechanical model in Figure 2.5.).

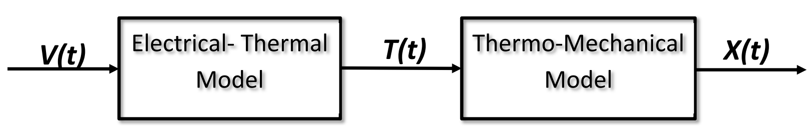

Figure 2.5: Block diagram for dynamic modeling with a dynamic voltage input $V(t)$.

For some TCAs made from conductive threads, the temperature increase is generated by current running through the actuator. Their conductivity makes them suitable for electrical actuated robotic systems. For such systems, the temperature can be predicted using an electrical-thermal model. If a voltage $V(t)$ is applied to the actuator, the model can be written as [22]:

$$C_t \frac{dT(t)}{dt} = \frac{V^2(t)}{R} - \lambda(T(t) - T_a) \tag{2.18}$$

where C_t is the thermal mass of the actuator, R is the resistance of the actuator, and λ is the absolute thermal conductivity for the actuator in its ambient environment, and T_a is the temperature of the ambient environment. In this equation, $V^2(t)/R$ is the energy injected to the actuator, while $\lambda(T(t) - T_a)$ is the energy dissipated to the ambient environment. Note that the resistance R will change depending on the temperature and displacement [42]; however, for simplicity, we assume the resistance be a constant.

2.5 Experimental Results

To verify our models, we conduct experiments and compare experimental results with simulation results obtained from the static and dynamic models. TCAs are fabricated using Shieldex Trading silver coated nylon sewing thread with a diameter of $0.17mm$ (117/17 2ply Silver Thread, PN: 260151011717oz). To fabricate the actuator, the thread's top end is vertically tied to a DC motor that rotates the thread, while a weight of 50 grams is hung at the bottom end to keep the fiber taut. This end is also constrained from rotation to allow twisting being inserted to the thread by the motor. After a sufficient number of twists, the twisted thread starts coiling, and the process ends until coils are formed along the thread. The final actuator has a diameter of 0.36 mm. The actuator is then annealed in a heating oven (Quincy Lab 20GC Aluminized Steel Hydraulic Gravity Convection Oven, 1.27 cubic feet) for 30 minutes at a temperature of $150°$ C. As a result, the actuator is stabilized and does not untwist when unloaded. Using a heating oven for annealing makes the fabricated actuators have consistent performances.

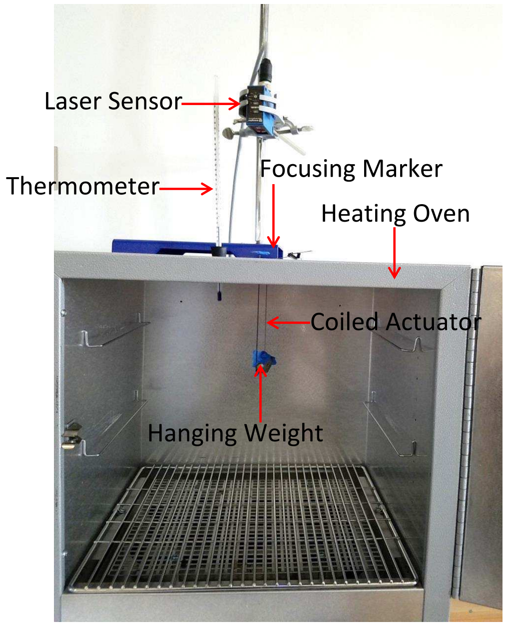

Figure 2.6: Experimental setup to verify the static model.

2.5.1 Results for Static Model

The static model is simulated using Matlab (Matlab® 2014b, The Mathworks Inc., Natick, MA) using the following procedure. The first step calculates the temperature induced torque τ using (2.9). In order to calculate τ, we need to determine the value of G_t using (2.12) or (2.13), which contains parameters like volume fraction V_f, fiber bias angle α_f and young's modulus E. V_f is calculated using $V_f = (r_f/r)^2 V_{fmax}$ [43], where $V_{fmax} = 0.887$ is the maximum possible volume fraction of fiber [43], r_f is the radius of filament and is taken as half of fiber radius r because the sewing thread used in our study is a 2ply (made out of two filaments) silver coated nylon thread. Fiber bias angle α_f is calculated using parameters *d* and ϕ. Young's modulus $E = 3.45GPa$ for Nylon 66 was taken from [44]. The other parameters in (2.9) include $l = 95mm$ and $\rho = -8.1 \times 10^{-5}k^{-1}$ [13, 38]. With all these parameters, the temperature induced torque is calculated for a known temperature change ΔT. The second step for simulation solves the pitch angle α using (2.10) and (2.11). Finally, we can solve the tensile actuation (contraction) of the coiled actuator for a given temperature change. The whole simulation procedure is repeated for a temperature range from 20°C to 150°C, and the results are shown in Figure 2.7 for a constant shear modulus computed by (2.12) (green curve) and varying shear modulus computed by (2.13) (red curve).

The experimental setup to verify the static model is shown in Figure 2.6. The same heating oven used for annealing the actuator is ulitilized to provide the increase of temperature. The coiled actuator is placed inside the oven with a weight of 50 grams attached to its bottom end. A laser displacement sensor (OPT2006, Wenglor photoelectric laser sensor) is placed outside of the oven to measure the displacement by focusing the laser spot onto a marker (weight od the marker has been accounted for) attached to the hanging weight in a way that it is parallel to the actuator so that it is displaced in a straight line during actuation. The chamber of the oven is heated with a temperature step of $5°$ C, and this temperature increment is measured using a thermometer inserted through a vent hole on the ceiling of the oven whereas the temperature is controlled using the temperature controlling knob on the oven. During the experiment, data from the laser sensor is sampled by an Arduino board. Data was recorded at each temperature increment of $5°$ C for a temperature range of $25°$ C to $150°$ C. Hence for each sample 26 data points were recorded.

Experimental results of the displacement versus temperature are also plotted in Figure 2.7 (blue curve) to compare with the modeling results. It can be seen that both modeling results can match the experimental results pretty well. Moreover, the modeling result with temperature dependent shear modulus is more accurate than that with a constant shear modulus, suggesting that we need to consider the change of shear modulus for better modeling results.

2.5.2 Results for Dynamic Model

To verify the dynamic model, we assume a weight is attached to the actuator's bottom end and a constant voltage is applied to the actuator. For this case, the dynamics model in (2.14) can be written as:

$$m\ddot{x} + b\dot{x} - mg + \frac{x - x_0 + f_{12}\tau}{f_{11}} = 0 \tag{2.19}$$

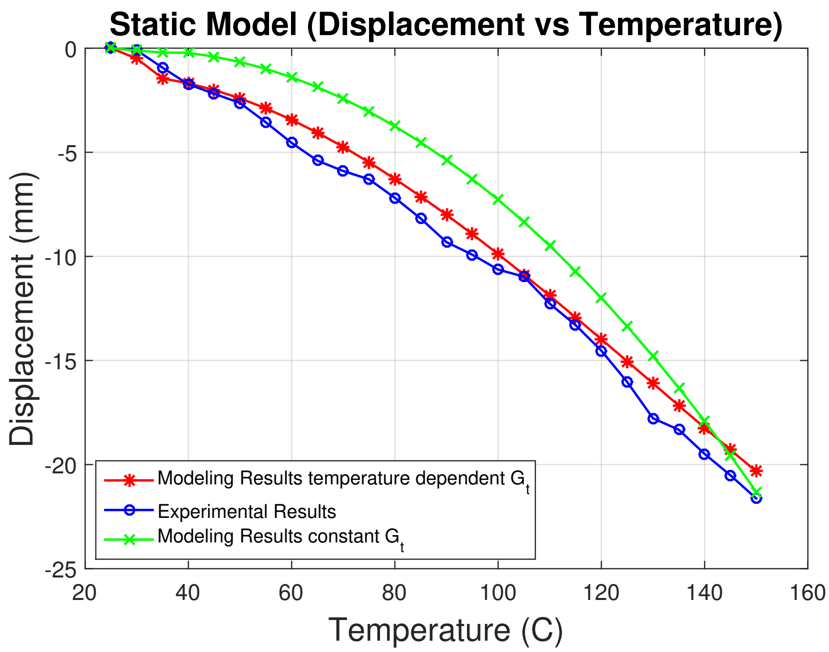

Figure 2.7: Simulation and experimental results for the static model.

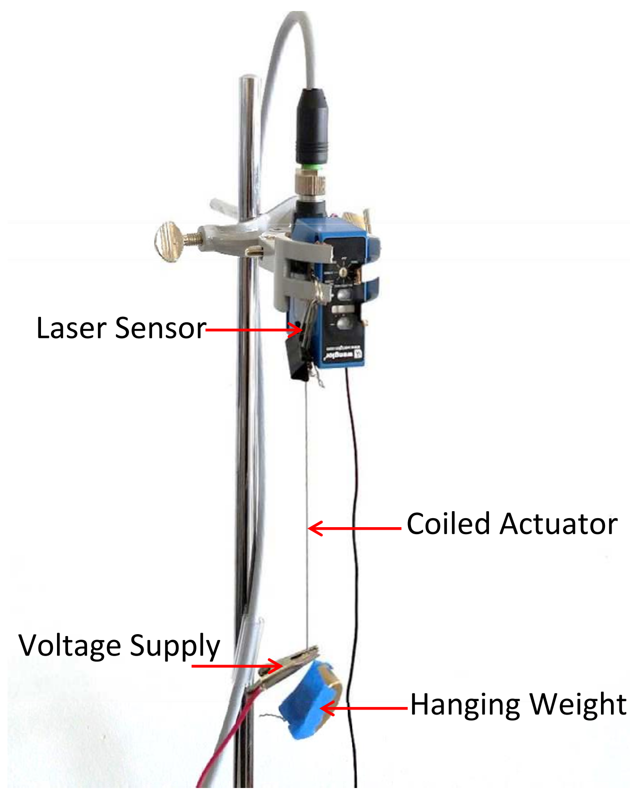

Figure 2.8: Experimental setup for dynamic model verification.

The dynamics model is also simulated in Matlab using the following procedure. First, we solve the electrical-thermal model (2.18) with a constant voltage input. The values for resistance of actuator R, constant voltage V, thermal mass C_{th}, absolute thermal conductivity λ, and ambient temperature T_a are 40 Ω, 10 volts, 0.0266 ± 0.00845 Ws/C°, 0.00893 ± 0.01615 W/C° and $20^{\circ}C$, respectively. It should be noted that all these values are for 95 mm long actuator and the values for C_{th} and λ are taken from [22] since similar material as [6] was used to fabricate the actuator. Even though the annealing techniques were different, but same temperature of $150^{\circ}C$ was applied, which is similar to [22] as they used application of a suitable voltage that could provide 0.2 $Watt/cm$ across the actuator which generates a temperature of $150^{\circ}C$. Once we obtain the increase in temperature as a function of time, we can solve the temperature induced torque to eventually solve the second order differential equation (2.19) and obtain the displacement as function of time. The value of damping coefficient *b* is chosen as 0.84 ± 0.12 [22]. The simulation result is plotted in blue color in Figure 2.9. For this plot, the varying shear modulus is ulitilized.

The experimental setup to verify our dynamic model uses the same laser displacement sensor and an actuator having the same parameters. Figure 2.8, shows the dynamic experimental setup. A weight of *50* grams is hung to the actuator and the temperature of the ambient environment is $20^{\circ}C$. The actuator is connected to a constant voltage source via wires (black at the top and red at the bottom end of the actuator) connected to alligator clips. The voltage is controlled through a motor driver (Pololu DC Motor Driver 3A, 5V-28V- MC33926), which allows us to apply a voltage of 10 volts for one second. This generates a quick reversible tensile actuation of the coiled actuator and the response is recorded by the laser sensor mounted at the top of the actuator. Again, the laser sensor data is sampled by an Arduino board, which also controls the motor driver.

The data obtained by laser sensor while the actuator contracts is plotted against time and compared with simulation results of our dynamic model. The plot is given in Figure 2.9, which shows similarity between experimental and modeling results. Especially the data points at the start and at the end of the curves are almost the same. We can therefore use this dynamic model to predict the actuator's displacement for closed-loop feedback control.

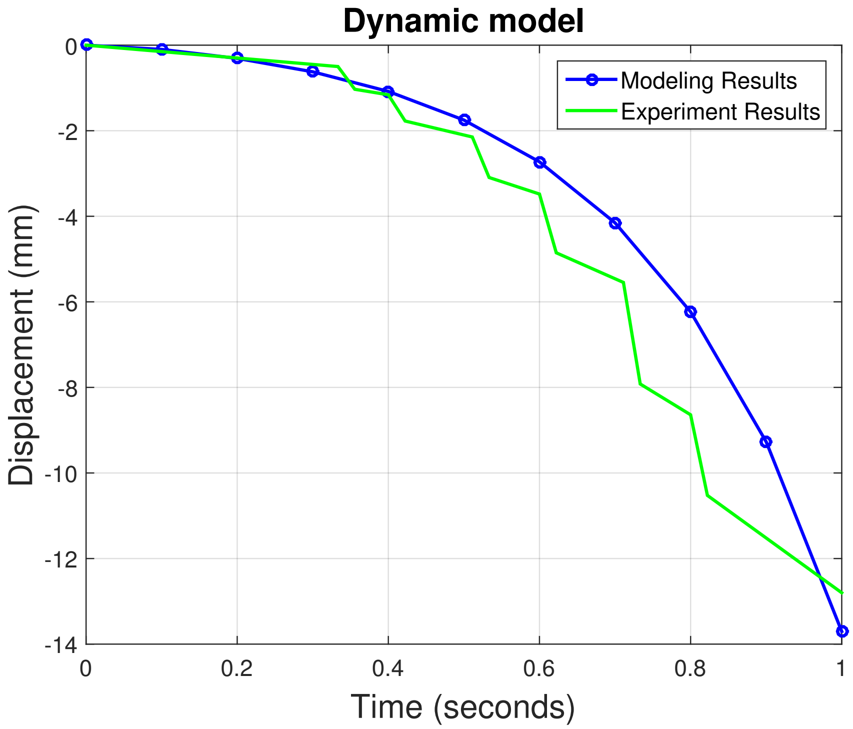

Figure 2.9: Simulation and experimental results for the dynamics model.

2.6 Conclusions

In this chapter we have established physics-based models to predict the static and dynamic response of twisted and coiled actuators (TCAs) made from polymer fibers. Compared with existing models, the proposed model is simple and can be applied to any TCAs if we know the material properties such as shear modulus, coefficient of thermal expansion, etc., and physical parameters such as initial length of twisted fiber, initial pitch angle of TCA, etc. Experimental results validate the proposed static and dynamics model, although some discrepancy exists.

Chapter 3

A Physics-Based Model for Twisted-and-Coiled Sensor

3.1 Introduction

It is difficult to precisely control soft robots' motion due to the infinite degrees of freedom accompanied with their soft body. Although tremendous efforts have been conducted to model the kinematics, statics, and dynamics of soft robots [2,45–48], closed-loop motion control is still in its early stage owing to the limitations of sensors to feedback a robot's shape in real-time [49].

Existing sensors for shape estimations of soft robots can be classified into two categories: external and internal sensors. External sensors are generally large systems placed outside the robot. With markers placed on a robot, external cameras can record images of soft robots and then reconstruct the shape from the markers' locations [3,20]. Electromagnetic sensors can be put on soft robots to obtain the position and orientation of several points to reconstruct the shape as well [21]. Although external sensors can provide accurate results, they are large and require either line-of-sight for cameras or special environments without magnetic objects for electromagnetic sensors.

Internal sensors are embedded into soft robots and can provide feedback without using external infrastructures [50]. Optical fibers are widely used for continuum robots [14] and soft robots [15, 16,51] to sense the strain as well as the torsion and force [52]. Liquid metal can be embedded into soft robots for curvature sensing of soft robots [17,18,53,54]. Other conductive material such as carbon black can also be added into elastomer material to enable conductive elastomer for shape estimation [55,56]. Miniature magnets and Hall-effect sensors have been embedded onto a flexible substrate to sense the curvature of soft robots [19].

Although many internal sensors have been developed, a major limitation for most of existing internal sensors is that they can only measure a single curvature for a circular shape of soft robots due to their working principle. In reality, however, soft robots can have arbitrarily three-dimensional shape, which cannot be described by a single curvature, and therefore cannot be measured using existing internal sensors.

To address such a limitation, this chapter aims to leverage the twisted-and-coiled artificial muscle (TCAM) as a sensor for soft robots. TCS has the following distinctive advantages. First and foremost, unlike existing internal sensors that can only sense one curvature, we can obtain as many curvatures as possible using TCS if we can measure the resistance for different sections in a single TCS. An example with two sections is shown in Figure 4.6. Second, as TCS was initially discovered as an actuator [13], we can design soft robots actuated by TCS and simultaneously estimate the shape to enable closed-loop control, potentially solving a challenging problem for soft robots. Third, TCS is economical and highly customizable. We can purchase them for prices as low as $\$0.3$ per meter [25]. Moreover, they are easy to fabricate, and customizations can be performed by changing the hanging weight during the fabrication process [13, 25].

There are two closely related work to the research presented in this chapter. First, the conductive yarn is leveraged for shape sensing of soft robots [57], but its resistance will decrease due to the lateral shrinkage of the yarn material in a stretchable pipe, whereas the resistance of a TCS will increase due to the decrease of the diameter in the twisted fiber. Second, the sensing capability of TCS is recently investigated [26], but the TCS is fabricated using a fishing line together with a conductive wire. Moreover, the developed models are based on simple curve fitting instead of from physics perspective.

Although we have investigated the sensing capability of TCS in [25], no theoretical model is provided for the sensor. The main contribution of this chapter is to provide a physics-based model using the physical parameters of a TCS to obtain both the force and displacement from the resistance.

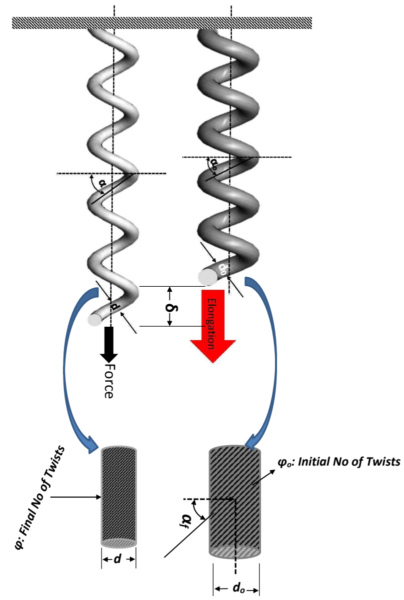

Figure 3.1: TCS on the right shows the initial configuration with the upper end fixed. Once an external force is applied to pull it, the length will increase but the diameter of the twisted fiber in the TCS will decrease as shown in the left TCS. This reduction in diameter causes the electrical resistance of the sensor to increase. The parameters shown are the initial diameter d_0 and pitch angle α_0 as well as current diameter d and pitch angle α when the force is applied. Bottom two figures show a small section of the twisted fiber with parameters labeled such as ϕ_0 and ϕ as well as the fiber bias angle α_f.

The rest of this chapter is organized as follows. Section 3.2 details the working principle as well as the theoretical modeling to predict force and change of length given the resistance. In section 3.3, an experimental setup is used to experimentally validate the theoretical models.

3.2 Modeling of Twisted and Coiled Sensors

The change of resistance for a twisted and coiled sensor (TCS) when it elongates is due to the decreased diameter of twisted fiber in the TCS. Since a TCS is fabricated by inserting twists and coils to it, the final TCS has a helical spring like structure. As observed under a microscope, neighboring coils will not contact each other after a TCS is fabricated. Therefore, the resistance for a TCS can be derived from the twisted fiber that formed the TCS:

$$R = \rho \frac{l}{A} \tag{3.1}$$

where l is the length for the twisted fiber in a TCS. ρ and A are the resistivity and cross sectional area for the conductive material in the twisted fiber, respectively. Note that conductive sewing thread is normally made from multiple silver coated nylon fibers. Therefore, we will use the resistivity of silver for ρ, which is a constant if the temperature is fixed. Moreover, l will only change slightly ($\sim 4\%$) [13], which is negligible. But since resistance will increase as the TCS elongates [25], the cross-section area A of silver inside the twisted fiber should decrease which is resulted from the decrease of diameter for twisted fiber. Suppose the initial diameter of a TCS is d_0 and the new diameter is d after a force is applied (Figure 3.1). In fact, once an external force is applied to stretch the sensor, and internal torque τ will be generated in the twisted fiber in a TCS to counter the external force. Such an internal torque will twist the fiber, and therefore decrease the diameter of the twisted fiber. Based on such a principle, we will establish a mathematical model to predict the change in length δ and the force F of a TCS provided the resistance R is known.

First, we solve the internal torque generated from the decrease of diameter. With a reasonable assumption that the area ratio between the silver and nylon in the cross-section area remains the same when an external force is applied, we have:

$$\frac{A}{A_0} = \left(\frac{d}{d_0}\right)^2 \tag{3.2}$$

where A_0 is the initial area of the silver, which can be derived from $A_0 = \rho l / R_0$ with R_0 the initial resistance. Similarly, A can also be derived from the current resistance $A = \rho l / R$. From this, we can solve for internal torque τ through (2.6), also given as (3.3):

$$\tau = \frac{G_t J \phi_0 (1 - d_0/d)}{l} \tag{3.3}$$

where all the parameters are for the twisted fiber. Specifically, G_t is the direction dependent shear modulus known as transverse shear modulus, $J = \pi d^4/32$ is the second moment of inertia, ϕ_0 is the initial number of twists inserted to the twisted fiber [13, 58], and d_0 is the initial diameter. The twisted fiber is an anisotropic polymer fiber, and therefore its mechanical properties are direction dependent [24]. We will use transverse shear modulus G_t which governs the shearing in the transverse plane because the radial contraction is in this plane. G_t is therefore given as [40]

$$G_t = \frac{4V_f E[\alpha_f/2 - \frac{1}{4}\sin(2\alpha_f)]^2}{\pi(2+\pi)(\frac{2}{3} - cos\alpha_f + \frac{1}{3}cos^3\alpha_f)(1-cos\alpha_f)} \tag{3.4}$$

where E is the Young's Modulus, V_f is the volume fraction of the fiber, and α_f is the fiber bias angle given as $\alpha_f = tan^{-1}(\pi d\phi)$ with ϕ the number of twists after elongation [13].

Once τ is solved, the next step of our model is to relate τ with displacement δ and external force F. Since a TCS has a helical spring-like structure, we can use a consistent spring model from Castigliano's Second Theorem [24, 39, 58], which relates the torque τ of the twisted fiber with the displacement δ and external force F of the TCS

$$\delta = f_{11}F - f_{12}\tau \tag{3.5}$$

where

$$\begin{aligned} f_{11} =& \frac{8n}{\pi^3 d^4}\left(\frac{l}{n}\right)^3 \frac{\cos^4\alpha}{G_t} + \frac{8n}{\pi d^2}\frac{l}{n}\frac{\cos^2\alpha}{2G_t} \\ &+ \frac{8n}{\pi^3 d^4}\left(\frac{l}{n}\right)^3 \frac{2\sin^2\alpha\cos^2\alpha}{E} + \frac{8n}{\pi d^2}\frac{l}{n}\frac{\sin^2\alpha}{2E} \\ f_{12} =& \frac{8n}{\pi^2 d^4}\left(\frac{l}{n}\right)^2 \frac{\cos^2\alpha}{G_t} \end{aligned}$$

In the above equation, n is the number of coils of the TCS given by $n = lcos\alpha_0/(\pi D)$, where D is the outside diameter of the TCS [13], α is the pitch angle for the TCS. The other parameters have been defined in the previous descriptions.

We have shown that the length of a TCS will increase linearly with the applied external force due to the spring-like structure [25], and has been observed by others as well [22]. Therefore, we leverage this property to relate the force and displacement via $F = S\delta$ in the static case, where S is the spring constant that can be experimentally identified and the procedure will be discussed in the later section. Therefore, (3.5) can be rewritten as:

$$\delta = f_{11} S\delta - f_{12}\tau \tag{3.6}$$

The displacement of a TCS can be related geometrically with the length l of the twisted fiber, initial pitch angle α_o and final pitch angle α of the TCS [58]:

$$\delta = l(\sin\alpha - \sin\alpha_0) \tag{3.7}$$

α_0 can be determined during the fabrication process as it is equal to the ratio between the coiled actuator length and twisted fiber length.

The two equations of δ (3.6) and (3.7) can then be solved simultaneously for the current pitch angle α. With the solved α, the displacement δ can be solved, from which we can also solve the external force F through $F = S\delta$.

3.3 Experimental Validations of Proposed Sensing Models

In order to verify our model, an experimental setup was developed (Figure 3.2) to measure the change in resistance and force with the changing length of a TCS. The setup consists of a linear actuator (Part #: L12-100-210-12-I, Actuonix) that is controlled by an Arduino board and has a force sensor (Part #: LSP-5, Transducer Techniques) at its moving end. One end of the TCS is tethered to the force sensor while the other end was fixed. A multimeter is hooked up with the TCS so that it could measure the resistance when the linear actuator pulls the TCS to elongate. The linear actuator is controlled in such a way that it moves $2mm$ in each step and then pauses for $5s$ so that the resistance change shown by the multimeter can be recorded. The increasing force is measured by the force sensor that is also hooked up with the Arduino board.

The fabrication process discussed in Section 2.2 and detailed in [25] was followed for TCS as well. We use silver coated nylon sewing threads from V Technical Textiles (Part #: 260151023534) with a diameter of *0.2 mm*. The hanging weight of *90* grams is adopted for fabrication. After

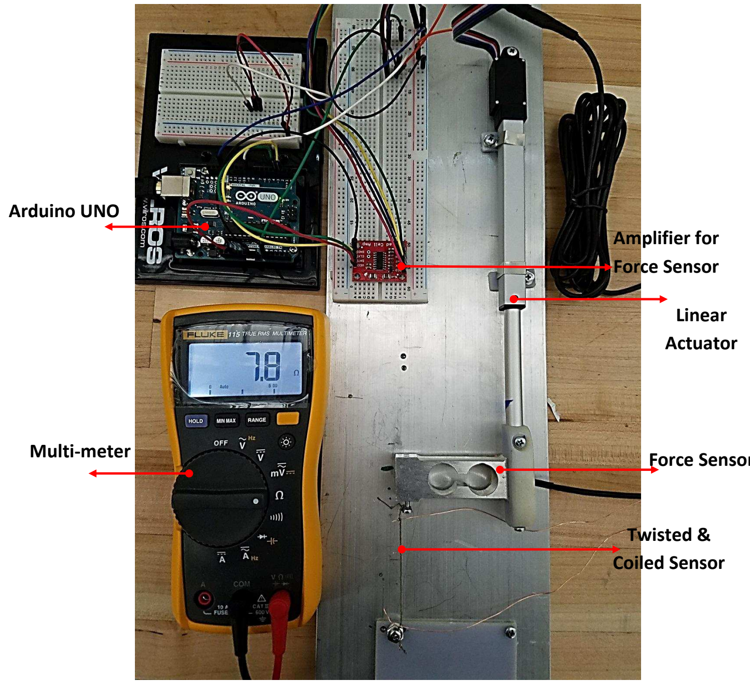

Figure 3.2: Experimental setup to measure the resistance, displacement, and force. TCS is mounted on this setup and pulled by a linear actuator; the force used to pull the TCS is measured by the force sensor and recorded by an Arduino board which is hooked to a laptop.

twisting and coiling this conductive thread, it is set in a heating oven for *60* minutes at a temperature of $150°$ Celsius.

The parameters to calculate the external force F and displacement δ using the proposed model are chosen as follows. The Youngs' modulus of Nylon 66 is E = *3.45 GPa*. The twisted fiber has a diameter of $d_0 = 0.4mm$ and number of twists $\phi_0 = 750$, which are measured during the fabrication process and are used to calculate initial α_f. Similarly, the twisted fiber length l = *328 mm*, TCS length L = *90 mm* and TCS diameter D = *0.8 mm* are measured during the fabrication process and used to calculate initial pitch angle α_0, number of coils n. V_f is calculated following the procedure in [58].

This experimental setup provides a data log that includes all the forces, resistances, and lengths of the TCS. The linear actuator elongates the TCS through a distance of 50 mm with an initial length of 90 mm. The curve between force and displacement is used to calculate the spring constant

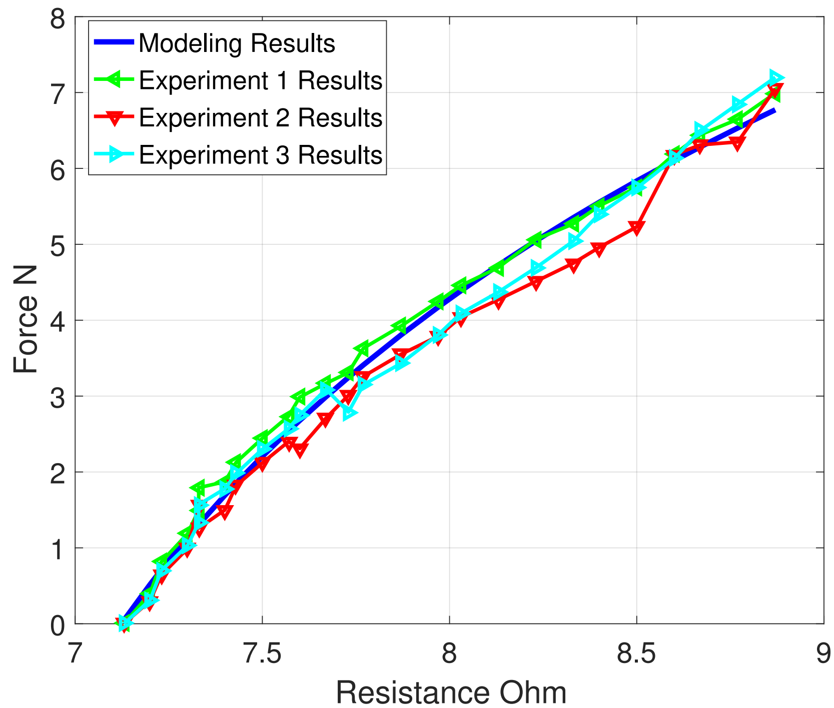

Figure 3.3: Plot shows the comparison between the modeling and experimental results for resistance vs force.

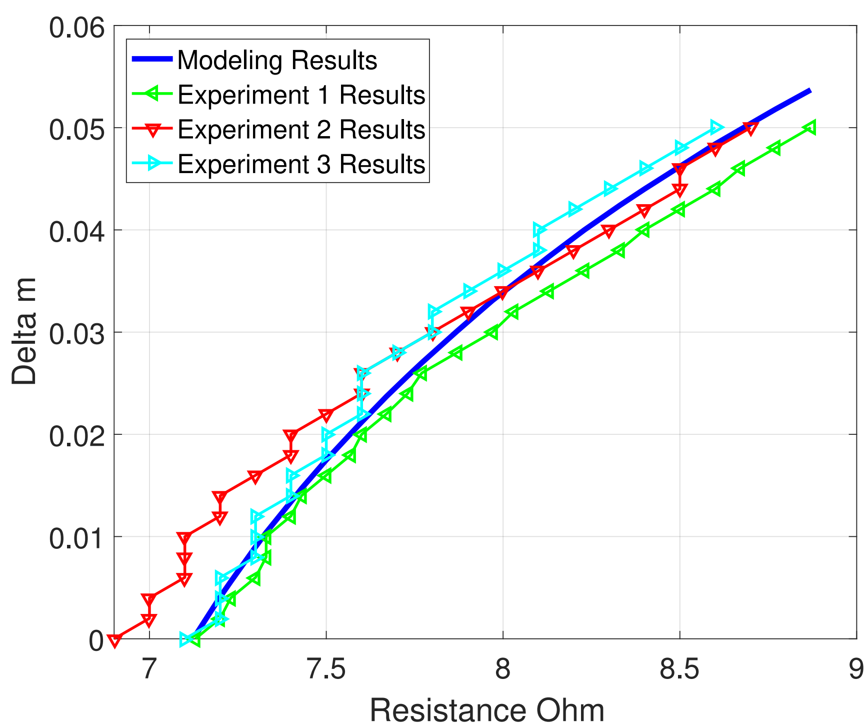

Figure 3.4: Plot shows the comparison between the modeling and experimental results for resistance vs displacement.

S using relation $F = S\delta$. Using all the data obtained from experiment, we can predict both the force and displacement using the mathematical model established in section 3.2.

The results for three experiments together with the modeling results are plotted in Figure 3.3 and Figure 3.4, where Figure 3.3, illustrates the force with respect to resistance, and Figure 3.4, is for the displacement with respect to resistance. From the two figures, we can see that the established model can predict both the force and displacement fairly well, although the initial values for the displacement in one of the distance results (Experiment 2 in Figure 3.4) is large.

3.4 CONCLUSIONS

In this chapter, we proposed a new soft sensor for the shape estimations of soft robots. The sensor can be made from conductive nylon sewing thread by continuously twisting the thread to eventually form coils. For TCS, its resistance will vary as the sensor's length changes. We have established a mathematical model to predict the change in displacement and external force if the resistance is known. The proposed model has been experimentally validated with a high precision. In the future, we will extend our model to include the temperature change, where the soft sensor's change in length and force can be predicted with known temperature and resistance. With such a model, we can also employ the sensor as an actuator for closed-loop control without using external sensing elements.

Chapter 4

Applications of Twisted and Coiled Artificial Muscle

4.1 Introduction

In the previous chapters, we have explored the actuation and the sensing aspects of the TCAM. In this chapter, we will discuss about the practical applications of TCAM. We will demonstrate that how a TCAM can be applied as an actuator and a sensor in soft robots. Most common actuators currently used are pneumatic actuators, hydraulic actuators or motor driven actuators. They have complicated design which makes the robot complicated in design as well. Similarly, the sensing mechanisms being currently used have a number of limitations. We have demonstrated through the application of TCAM, that when used as an actuator or as a sensor it does not have such limitations.

4.2 Applications of TCA

Twisted and coiled actuator has number of advantages over the actuators that are being currently used in soft robotics. We will revise the five major advantages of TCA here. First, they can generate life like motions which is particularly useful in humanoid robots. Second, TCAs do not require bulky parts like valves and pumps for their actuation, this allows us to simplify the design of the soft robot. Third, they can be easily embedded inside a soft robot as can be seen in Figure 4.2 and Figure 4.4. Fourth, they do not need any special environment for their operation, Figure 4.2, shows that a TCA fabricated following the method discussed earlier can also be operated underwater. Fifth, they are very low cost and can be easily fabricated with a great deal of customization. In this thesis, we have used these advantages of the TCA and applied them in two different robotic applications. A fish tail robot that can actuate under water and a simple robotic finger. The fabrication methods and the actuation cycles of these robots are discussed in following sections.

4.2.1 Robotic Fish Tail

In this application we will demonstrate the actuation of a robotic fishtail underwater using the TCA. The fabrication of the robot is simple and has been briefly shown in Figure 4.1a. In the first step TCAs are mounted inside the 3D printed mold, which is made in two halves. A total of six similar TCAs are placed in the mold at three different locations. Each location has two TCAs placed parallel to each other in a way that the distance of each TCA from the center of the fish tail is the same. This will allow the fish tail to bend (either left or right) towards the side of the TCAs that are being actuated. After fitting the TCAs, the molds are joined together and mounted on the base mold which is shown in Figure 4.1b. The base becomes an integral part of the fish tail once the soft robot is extracted. After joining the three mold parts together, a curable soft material EcoFlex 00-10 [59], is poured in the mold through the holes provided at the top. The material is then left to cure for four to five hours. After the soft material is completely cured, the fish tail robot is extracted by removing the upper two halves from the base. Figure 4.1b, shows how the fish tail robot looks after extraction.

After fabrication is completed, the TCAs on left side are connected electrically in parallel, similarly TCAs on the right are also connected. After ensuring that the connections are good, the TCAs are hooked-up with a power supply that will provide with a DC voltage. A voltage of 10 volts is applied to one side of the tail, i.e. either left TCAs or right TCAs. The voltage generates Joule heating effect across the TCAs and make them actuate, as a result the fish tail is actuated under water. The actuation cycle of the fish tail under water is shown in Figure 4.2.

4.2.2 Robotic Finger

One of the advantages of the TCA is that it can mimic the motion of a biological muscle. Hence we have applied this natural life like motion in a robotic finger shown in Figure 4.4. The fabrication process is similar to the one used to make fish tail. The mold that was used to fabricate the robotic finger is shown in Figure 4.3. The design of the finger is such that three TCAs were embedded at 120^o each. The actuation cycle shown in Figure 4.4, was achieved by actuating one of the three

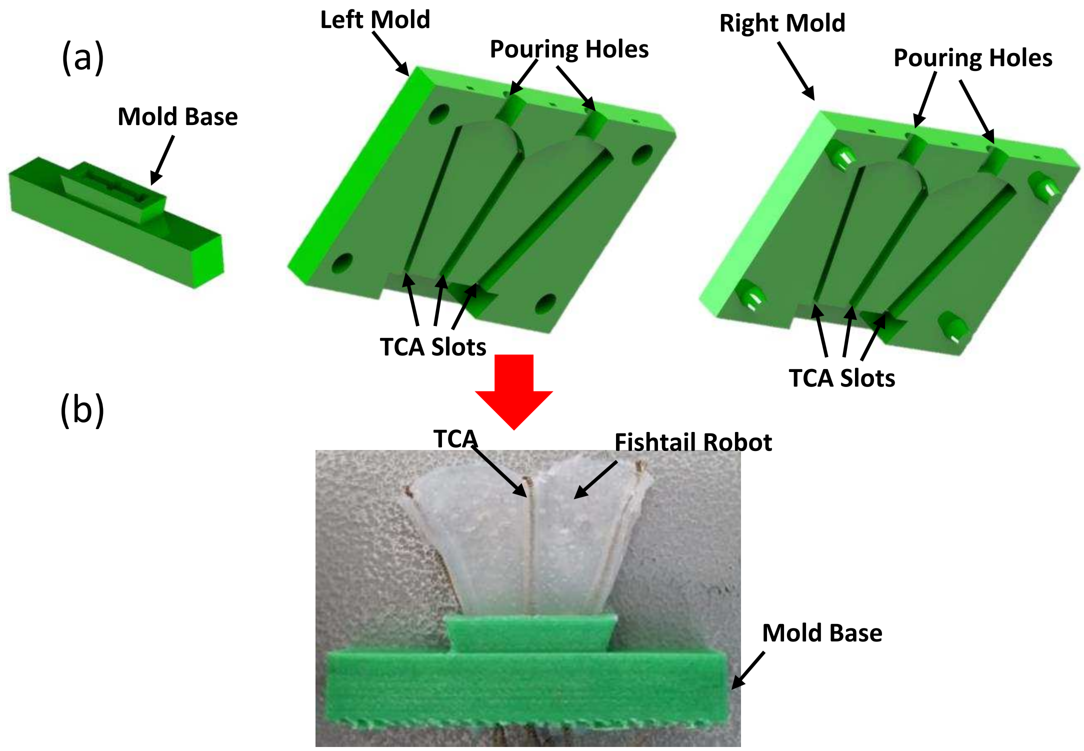

Figure 4.1: Fabrication of fish tail robot. (a) 3D printed mold which has three parts; mold base, left mold and right mold. These parts are joined together and TCAs are mounted inside the mold at their designated positions. EcoFlex 00-10 is then poured into the mold and left to cure. (b) Fish tail robot that is extracted out of the mold after the soft material inside is allowed to cure for four to five hours.

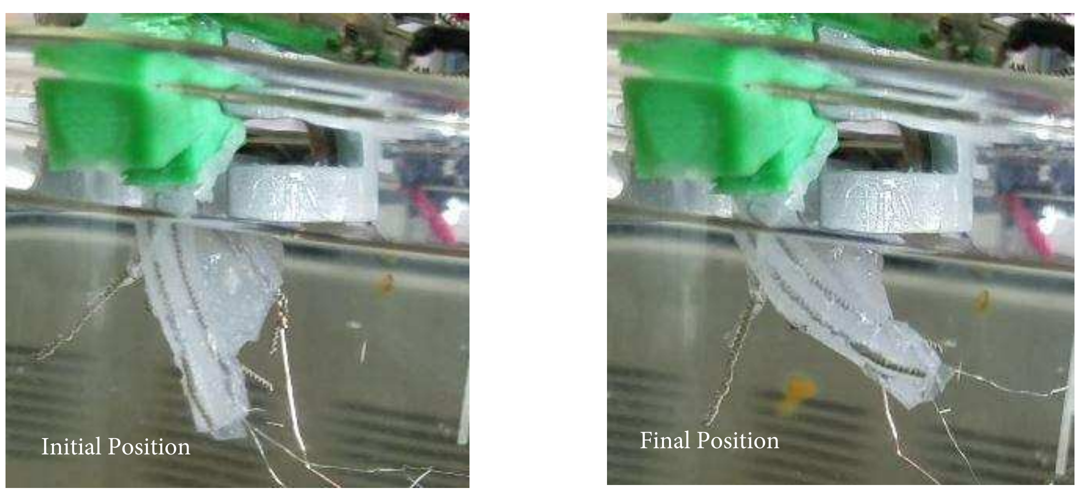

(a) (b)

Figure 4.2: Actuation of fish tail robot underwater. (a) Initial position when power supply is off. (b) Final position when the TCA actuates the fish tail.

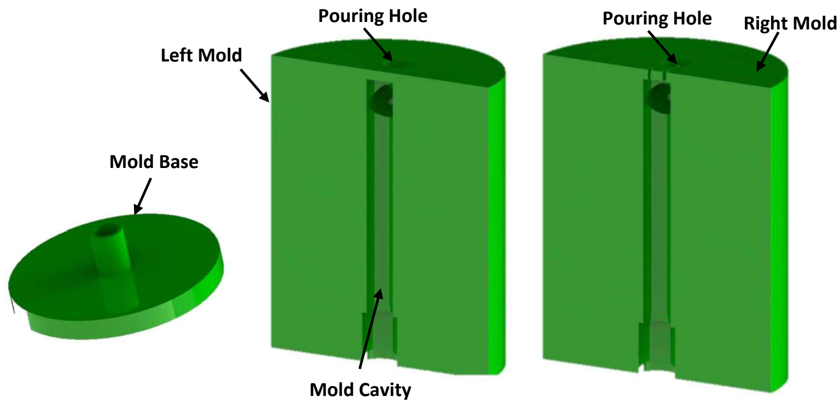

Figure 4.3: 3D printed molds used for the fabrication of soft robotic finger. The soft robotic finger extracted from this mold is shown in Figure 4.4.

TCAs. The same power supply from the fish tail actuation was used and a voltage of 10 volts was applied to the TCA. A bending angle of approximately 90^o was achieved and can be also seen in Figure 4.4.

4.3 Application of TCS

To demonstrate the capability of TCAM as a sensor, we embedded TCS into a soft robot made from two soft materials Figure 4.6. The bottom half of the robot is made from EcoFlex 00-30 (Smooth-On) and its tensile strength is 1.4 *MPa* [60], whereas the top half is made from EcoFlex 00-10, which, softer than EcoFlex 00-30, has a tensile strength of 0.8 *MPa* [59]. With different stiffness in the two segments, the robot exhibits two different curvatures if pulled by a cable embedded inside the robot. Hence, different from existing sensors, we show that TCS can be leveraged to estimate two curvatures, which can be readily applied to the estimation of many curvatures, leading to the possibility of estimating any arbitrary shape.

The fabrication process shown in Figure 4.5 is utilized to fabricate the soft robot shown in Figure 4.6. First, we design a 3D printed mold with a cavity being the shape of our soft robot with two holes on front and end side to fix the TCS and pulling cable Figure 4.5a. Second, a TCS and a silicone tube are mounted inside the mold at symmetrical locations with respect to the center of the mold Figure 4.5b. The cable is then placed inside the silicone tube. Moreover, three

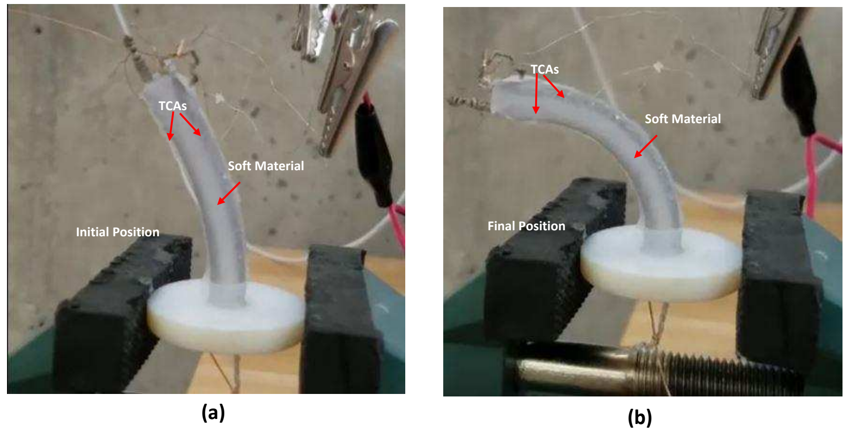

Figure 4.4: The actuation of soft robotic finger. (a) Initial position of the finger when power supply is off. (b) Final position when the TCA actuates the finger.

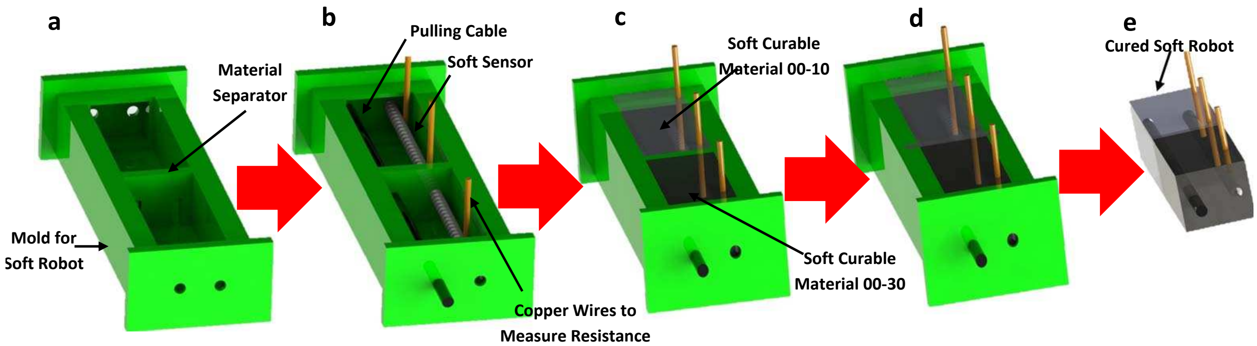

Figure 4.5: The fabrication process of soft robot with embedded twisted and coiled sensors.

copper wires are connected to the sensor with the second one located at the center. These wires will be used to measure the resistance via multimeter that can be attached to these wires. Third, EcoFlex 00-30 and EcoFlex 00-10 are poured into their respective halves Figure 4.5c. The mold is designed to keep these liquids but curable materials from mixing with each other during pouring with a 3D printed separator. Fourth, once the pouring is completed, the separator is removed from the mold Figure 4.5d so that after curing we get a single multi-material soft robot. Finally, after approximately 5 hours of curing, the soft robot is extracted out of the mold for experiments Figure 4.5e. The final robot has a size of $60mm \times 12mm \times 10mm$.

For this soft robot, three copper wires on the TCS divide the whole robot into two segments. We can use the resistance R_1 to estimate the curvature for the first segment (top half made of EcoFlex 00-10), and R_2 for the curvature of the second segment (bottom half made of EcoFlex 00-30). It

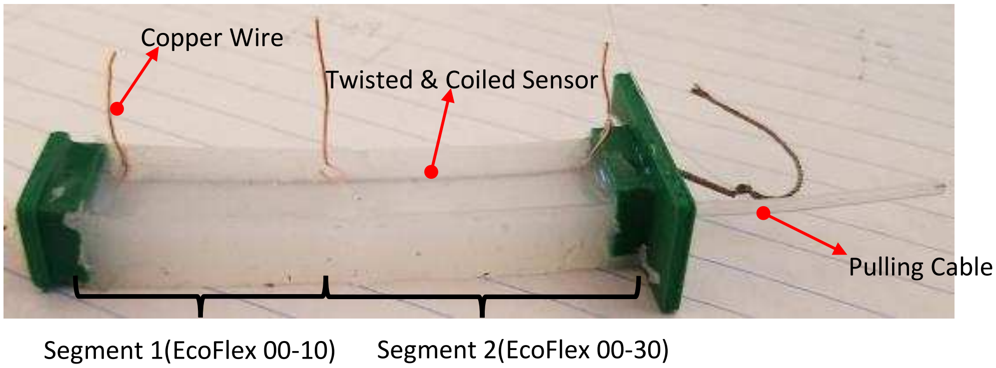

Figure 4.6: A soft robot with an embedded twisted and coiled sensor (TCS) and a pulling cable to bend it. (Note that as a TCS is embedded inside the soft robot and cannot be clearly shown. The green rigid parts at both ends are used to fix the robot and the pulling cable.).

should be noted that more wires can be added to measure the curvature of more segments, although we only used three wires to illustrate the idea.

To demonstrate the capability of shape estimation using the fabricated soft robot, we continuously bend the robot by pulling the cable and sampling the resistance for all the configurations. Experimental setup shown in Figure 3.2 is again used, but the soft coiled sensor is replaced by the cable embedded in the robot. We pull the cable to a displacement of 2 *mm* in each step. For this approach, ground truth of the curvature is obtained using a camera to capture the image of each bending configuration of the robot. These images are then processed using Matlab to get the curvatures of two segments [61]. The resistances R_1 and R_2 for each configuration are measured using two multimeters that are attached to the three copper wires tied. These resistances are utilized to estimate the corresponding length using our mathematical model developed in Chapter 3. Finally, the lengths are used to calculate the corresponding curvature of each segment using the following equation as the angle θ is same for both C_1 and C [25]:

$$K = \frac{C_1 - C}{C d_1} \tag{4.1}$$

where C_1 is the length of the soft sensors (Note that the soft sensor elongates when the cable bends the robot), C is the length of the cable inside the robot, $d_1 = 9$ *mm* is the distance of the sensors from the cable. The estimated and experimental curvature for two segments are plotted in

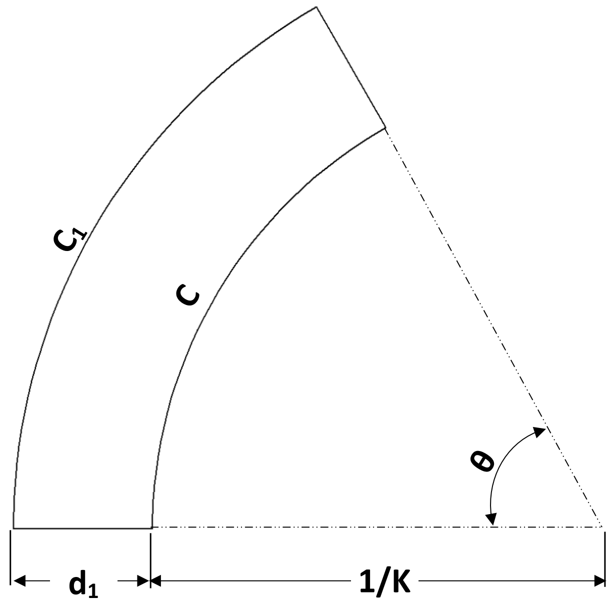

Figure 4.7: Schematic showing curvature of one of the segments of the soft robot.

Figure 4.7. As can be seen from the figure, the curvature can be closely estimated from the two resistances

with the curvature of top segment being larger than that of bottom segment, which is correct since the material at the top is softer than the bottom. There is some large error for some points, which might be because the bending of the soft robot cannot be perfectly described by a circular shape since axial compression cannot be neglected. Further, using images from a camera to obtain the curvature might have some errors resulted from the inaccurate placement of the camera.

4.4 Conclusions

In this chapter, we have discussed the practical applications of the TCAMs as actuator and sensor. This low cost soft actuator can be embedded in a soft robot and can be stimulated to generate life like motion. TCA because of the simplicity in its design and fabrication also allow us to keep the design and fabrication of soft robotic systems simple. Which can be seen from the two very simple and easy to fabricate soft robots that we have used. We have also used the self-sensing capability of the TCAM and demonstrated the multi-curvature shape estimation of a soft robot. The modeling results were verified by comparing them with the experimental results and a great

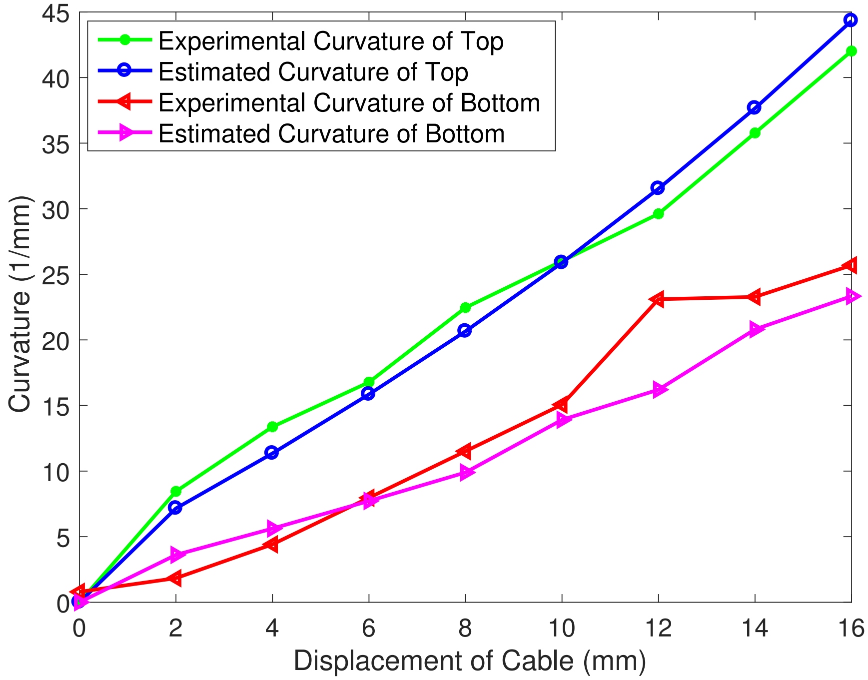

Figure 4.8: Plot shows estimated and experimental curvatures of both the halves of soft robot.

deal of accuracy can be seen. In future, the actuation and sensing capability of the TCAM can be combined, so that the TCAM can be used as the actuator and internal sensor at the same time. This will allow us to implement closed loop control and hence the motion of the robot can be controlled precisely.

Chapter 5

Conclusions and Future Work

5.1 Conclusions

In this thesis, we have studied the actuation and the sensing characteristics of the TCAM. They have the potential to replace the actuators and sensors that are being currently used in the soft robots. As discussed in Chapter 1, a traditional rigid bodied robot has fixed degree of freedom and in most cases, can only perform single task with dexterity. Whereas, soft robots have inherently soft and flexible bodies. This allows them to exhibit unprecedented adaptation, sensitivity and agility. Soft robots have the ability to twist and bend with high degrees of freedom, they can therefore be used in confined spaces and uncertain environments. Based on the differences between traditional and soft robots, the actuators used in soft robots should be different than the rigid traditional actuators. A soft actuator embedded inside a soft robot helps to make the actuation more efficient, since the actuation occurs within the body. Unlike the actuation in a traditional actuator, where the mechanical power is propagated from a different source into the robot, e.g. compressed air traveling form a compressor into soft robot in case of pneumatic actuators. A soft actuator does not have bulky parts like valves and motors, it therefore helps to simplify the design of a robot.

We have therefore demonstrated a soft artificial muscle actuator TCAM that has a twisted and coiled configuration. Like soft robots, TCAM also has compliant structure and can be embedded inside a soft robot. We have also developed a physics based mathematical model that can predict both the static and dynamic actuation response of the TCA. Two experimental setups were designed and developed to capture the static and dynamic actuation response of the TCA. The experimental results obtained were compared with the modeling results. The comparisons show that our model can precisely determine the actuation response of the TCA when the actuation is induced by temperature.

Another major advantage of the TCAM that we have demonstrated is its ability to work as a sensor. The soft sensor termed as TCS is made from silver coated nylon sewing thread and is therefore conductive. The resistance of TCS changes when the it elongates. Hence when it is embedded inside a soft robot it provides with the change in its resistance and this information is effectively used to estimate the shape of the robot. One of the major advantages of TCS over existing sensors is that it can estimate the shape change of the robot that bends with multiple curvatures. Whereas, the existing sensors can only estimate a single curvature of the robot. To harness the self-sensing potential of the TCS we have developed a sensing model that uses the change in resistance of the TCS and calculates the curvature(s) of the bending robot. Our model can also predict the external force applied to the TCS and the change in displacement with respect to resistance change. The precision of our model can be seen from the comparison between experimental and modeling results.

We have also used TCAM in robotic applications. We have shown two different soft robots, a robotic finger and a robotic fishtail. Both these robots are actuated using TCA that were developed by following the fabrication process discussed in Chapter 2. We have also demonstrated the sensing ability of the TCAM by embedding it in a soft robot and using its resistance change in our sensing model to estimate the shape change of a multiple-curvature robot. The results obtained show that our model and the TCS are both precise in estimating the shape change of the robot.

5.2 Future Work

In future, we intend to combine both the actuation and sensing aspects of the TCAM; so that it can be embedded in a soft robot and can work as an actuator and as a sensor at the same time. The actuation model that we have developed provides us with the temperature induced actuation of the TCA. Whereas, the sensing model predicts the shape change of the robot by using the resistance change of the TCS. In order to combine actuation and sensing, we need to come up with a more sophisticated sensing model. One that includes the effect of temperature on the resistance of the TCS. Whereas, the existing model can only comprehend the resistance change of the TCS when it is elongated mechanically at constant temperature. But in reality, when actuation and sensing is combined, the actuation of the TCS will be temperature induced. Once such a model is developed, we will be able to use TCAM as one unit that can actuate and also sense the shape of the robot in which it has been embedded. This will provide the means of closed-loop control of the soft robot without using external sensors.

Bibliography

[1] TechGen. Soft Robotic Hand url(https://www.http://techgenmag.com/2014/07/soft-robotics/).

[2] Andrew D Marchese, Russ Tedrake, and Daniela Rus. Dynamics and trajectory optimization for a soft spatial fluidic elastomer manipulator. *The International Journal of Robotics Research*, 35(8):1000–1019, 2016.

[3] Andrew D Marchese and Daniela Rus. Design, kinematics, and control of a soft spatial fluidic elastomer manipulator. *The International Journal of Robotics Research*, 35(7):840–869, 2016.

[4] Michael T Tolley, Robert F Shepherd, Bobak Mosadegh, Kevin C Galloway, Michael Wehner, Michael Karpelson, Robert J Wood, and George M Whitesides. A resilient, untethered soft robot. *Soft Robotics*, 1(3):213–223, 2014.

[5] Cagdas D Onal and Daniela Rus. Autonomous undulatory serpentine locomotion utilizing body dynamics of a fluidic soft robot. *Bioinspiration & biomimetics*, 8(2):026003, 2013.

[6] Andrew D Marchese, Cagdas D Onal, and Daniela Rus. Autonomous soft robotic fish capable of escape maneuvers using fluidic elastomer actuators. *Soft Robotics*, 1(1):75–87, 2014.

[7] B Mazzolai, L Margheri, M Cianchetti, P Dario, and C Laschi. Soft-robotic arm inspired by the octopus: Ii. from artificial requirements to innovative technological solutions. *Bioinspiration & biomimetics*, 7(2):025005, 2012.

[8] Seyed M Mirvakili, Alexey Pazukha, William Sikkema, Chad W Sinclair, Geoffrey M Spinks, Ray H Baughman, and John DW Madden. Niobium nanowire yarns and their application as artificial muscles. *Advanced Functional Materials*, 23(35):4311–4316, 2013.

[9] Ailish OâĂŹHalloran, Fergal OâĂŹmalley, and Peter McHugh. A review on dielectric elastomer actuators, technology, applications, and challenges. *Journal of Applied Physics*, 104(7):071101, 2008.

[10] Mohsen Shahinpoor, Y Bar-Cohen, JO Simpson, and J Smith. Ionic polymer-metal composites (ipmcs) as biomimetic sensors, actuators and artificial muscles-a review. *Smart materials and structures*, 7(6):R15, 1998.

[11] Choonghee Jo, David Pugal, Il-Kwon Oh, Kwang J Kim, and Kinji Asaka. Recent advances in ionic polymer–metal composite actuators and their modeling and applications. *Progress in Polymer Science*, 38(7):1037–1066, 2013.

[12] Jaronie Mohd Jani, Martin Leary, Aleksandar Subic, and Mark A Gibson. A review of shape memory alloy research, applications and opportunities. *Materials & Design*, 56:1078–1113, 2014.

[13] Carter S Haines, Márcio D Lima, Na Li, Geoffrey M Spinks, Javad Foroughi, John DW Madden, Shi Hyeong Kim, Shaoli Fang, Mônica Jung de Andrade, Fatma Göktepe, et al. Artificial muscles from fishing line and sewing thread. *Science*, 343(6173):868–872, 2014.

[14] Roy J Roesthuis, Sander Janssen, and Sudip Misra. On using an array of fiber bragg grating sensors for closed-loop control of flexible minimally invasive surgical instruments. In *Intelligent Robots and Systems (IROS), 2013 IEEE/RSJ International Conference on*, pages 2545–2551, 2013.

[15] Sina Sareh, Yohan Noh, Min Li, Tommaso Ranzani, Hongbin Liu, and Kaspar Althoefer. Macrobend optical sensing for pose measurement in soft robot arms. *Smart Materials and Structures*, 24(12):125024, 2015.

[16] Huichan Zhao, Kevin OâĂŹBrien, Shuo Li, and Robert F Shepherd. Optoelectronically innervated soft prosthetic hand via stretchable optical waveguides. *Sci. Robot.*, 1(1):eaai7529, 2016.

[17] Yong-Lae Park, Bor-Rong Chen, and Robert J Wood. Design and fabrication of soft artificial skin using embedded microchannels and liquid conductors. *Sensors Journal, IEEE*, 12(8):2711–2718, 2012.

[18] Nicholas Farrow and Nikolaus Correll. A soft pneumatic actuator that can sense grasp and touch. In *Intelligent Robots and Systems (IROS), 2015 IEEE/RSJ International Conference on*, pages 2317–2323, 2015.

[19] Selim Ozel, Nehir A Keskin, Darien Khea, and Cagdas D Onal. A precise embedded curvature sensor module for soft-bodied robots. *Sensors and Actuators A: Physical*, 236:349–356, 2015.

[20] M Giorelli, F Renda, M Calisti, A Arienti, G Ferri, and C Laschi. Learning the inverse kinetics of an octopus-like manipulator in three-dimensional space. *Bioinspiration & biomimetics*, 10(3):035006, 2015.

[21] Shuang Song, Zheng Li, Haoyong Yu, and Hongliang Ren. Electromagnetic positioning for tip tracking and shape sensing of flexible robots. *Sensors Journal, IEEE*, 15(8):4565–4575, 2015.

[22] Michael C Yip and Gunter Niemeyer. High-performance robotic muscles from conductive nylon sewing thread. In *Robotics and Automation (ICRA), 2015 IEEE International Conference on*, pages 2313–2318, 2015.

[23] Takeshi Arakawa, Kentaro Takagi, Kenji Tahara, and Kinji Asaka. Position control of fishing line artificial muscles (coiled polymer actuators) from nylon thread. In *SPIE Smart Structures and Materials+ Nondestructive Evaluation and Health Monitoring*, pages 97982W–97982W, 2016.

[24] Qianxi Yang and Guoqiang Li. A top-down multi-scale modeling for actuation response of polymeric artificial muscles. *Journal of the Mechanics and Physics of Solids*, 92:237–259, 2016.

[25] Jianguo Zhao and Ali Abbas. A low-cost soft coiled sensor for soft robots. In *ASME 2016 Dynamic Systems and Control Conference*, pages V002T26A006–V002T26A006. American Society of Mechanical Engineers, 2016.

[26] Joost van der Weijde, Bram Smit, Michael Fritschi, Cornelis van de Kamp, and Heike Vallery. Self-sensing of deflection, force, and temperature for joule-heated twisted and coiled polymer muscles via electrical impedance. *IEEE/ASME Transactions on Mechatronics*, 22(3):1268–1275, 2017.

[27] Lokesh Saharan and Yonas Tadesse. Robotic hand with locking mechanism using tcp muscles for applications in prosthetic hand and humanoids. In *SPIE Smart Structures and Materials+ Nondestructive Evaluation and Health Monitoring*, pages 97970V–97970V, 2016.

[28] Ankit Tomar and Yonas Tadesse. Multi-layer robot skin with embedded sensors and muscles. In *SPIE Smart Structures and Materials+ Nondestructive Evaluation and Health Monitoring*, pages 979809–979809, 2016.

[29] Kyeong Ho Cho, Min Geun Song, Hosang Jung, Jungwoo Park, Hyungpil Moon, Ja Choon Koo, Jae-Do Nam, and Hyouk Ryeol Choi. A robotic finger driven by twisted and coiled polymer actuator. In *SPIE Smart Structures and Materials+ Nondestructive Evaluation and Health Monitoring*, pages 97981J–97981J, 2016.

[30] Lianjun Wu, Monica Jung de Andrade, Tarang Brahme, Yonas Tadesse, and Ray H Baughman. A deformable robot with tensegrity structure using nylon artificial muscle. In *SPIE Smart Structures and Materials+ Nondestructive Evaluation and Health Monitoring*, pages 97993K–97993K. International Society for Optics and Photonics, 2016.

[31] Hongda Li, Long Liu, Tianhang Xiao, and Haisong Ang. Design and simulative experiment of an innovative trailing edge morphing mechanism driven by artificial muscles embedded in skin. *Smart Materials and Structures*, 25(9):095004, 2016.

[32] Lee Sutton, Hadi Moein, Ali Rafiee, John DW Madden, and Carlo Menon. Design of an assistive wrist orthosis using conductive nylon actuators. In *2016 6th IEEE International Conference on Biomedical Robotics and Biomechatronics (BioRob)*, pages 1074–1079. IEEE, 2016.

[33] Seyed M Mirvakili and Ian W Hunter. Bending artificial muscle from nylon filaments. In *SPIE Smart Structures and Materials+ Nondestructive Evaluation and Health Monitoring*, pages 97981L–97981L, 2016.

[34] Michael C Yip and Günter Niemeyer. On the control and properties of super-coiled polymer artificial muscles. *IEEE Transactions on Robotics*, To Appear, 2016.

[35] Shazed Aziz, Sina Naficy, Javad Foroughi, Hugh R Brown, and Geoffrey M Spinks. Controlled and scalable torsional actuation of twisted nylon 6 fiber. *Journal of Polymer Science Part B: Polymer Physics*, 54(13):1278–1286, 2016.

[36] John Case and Amos Henry Chilver. *Strength of materials and structures: an introduction to the mechanics of solids and structures*. Elsevier, 2013.

[37] C Pradere and C Sauder. Transverse and longitudinal coefficient of thermal expansion of carbon fibers at high temperatures (300–2500k). *Carbon*, 46(14):1874–1884, 2008.

[38] Hiroyuki Kikuchi and Kiyohito Koyama. Material anisotropy and warpage of nylon 66 composites. *Polymer Engineering & Science*, 34(18):1411–1418, 1994.

[39] Clive L Dym. Consistent derivations of spring rates for helical springs. *Journal of Mechanical Design*, 131(7):071004, 2009.

[40] Ning Pan and David Brookstein. Physical properties of twisted structures. ii. industrial yarns, cords, and ropes. *Journal of applied polymer science*, 83(3):610–630, 2002.

[41] Soodabeh Sharafi and Guoqiang Li. A multiscale approach for modeling actuation response of polymeric artificial muscles. *Soft matter*, 11(19):3833–3843, 2015.

[42] Jianguo Zhao and Ali Abbas. A low cost soft coiled sensor for soft robots. In *ASME Dynamic Systems and Control Conference (DSCC)*, page To appear, 2016.

[43] Magdi El Messiry. Theoretical analysis of natural fiber volume fraction of reinforced composites. *Alexandria Engineering Journal*, 52(3):301–306, 2013.

[44] Tsu-Wei Chou. *Microstructural design of fiber composites*. Cambridge University Press, 2005.

[45] Joshua Bishop-Moser and Sridhar Kota. Design and modeling of generalized fiber-reinforced pneumatic soft actuators. *IEEE Transactions on Robotics*, 31(3):536–545, 2015.

[46] Panagiotis Polygerinos, Zheng Wang, Johannes TB Overvelde, Kevin C Galloway, Robert J Wood, Katia Bertoldi, and Conor J Walsh. Modeling of soft fiber-reinforced bending actuators. *IEEE Transactions on Robotics*, 31(3):778–789, 2015.

[47] Isuru S Godage, Gustavo A Medrano-Cerda, David T Branson, Emanuele Guglielmino, and Darwin G Caldwell. Dynamics for variable length multisection continuum arms. *The International Journal of Robotics Research*, 35(6):695–722, 2016.

[48] Michele Giorelli, Federico Renda, Marcello Calisti, Andrea Arienti, Gabriele Ferri, and Cecilia Laschi. Neural network and jacobian method for solving the inverse statics of a cable-driven soft arm with nonconstant curvature. *IEEE Transactions on Robotics*, 31(4):823–834, 2015.

[49] Jennifer C Case, Edward L White, and Rebecca K Kramer. Sensor enabled closed-loop bending control of soft beams. *Smart Materials and Structures*, 25(4):045018, 2016.

[50] Morteza Amjadi, Ki-Uk Kyung, Inkyu Park, and Metin Sitti. Stretchable, skin-mountable, and wearable strain sensors and their potential applications: A review. *Advanced Functional Materials*, 2016.

[51] Sina Sareh, Y Noh, T Ranzani, H Wurdemann, H Liu, and K Althoefer. A 7.5 mm steiner chain fibre-optic system for multi-segment flex sensing. In *IEEE/RSJ International Conference on Intelligent Robots and Systems (IROS)*, pages 2336–2341, 2015.

[52] R. Xu, A. Yurkewich, and R. V. Patel. Curvature, torsion, and force sensing in continuum robots using helically wrapped fbg sensors. *IEEE Robotics and Automation Letters*, 1(2):1052–1059, 2016.

[53] Stefania Russo, Tommaso Ranzani, Hongbin Liu, Samia Nefti-Meziani, Kaspar Althoefer, and Arianna Menciassi. Soft and stretchable sensor using biocompatible electrodes and liquid for medical applications. *Soft Robotics*, 2(4):146–154, 2015.

[54] C Majidi, R Kramer, and RJ Wood. A non-differential elastomer curvature sensor for softer-than-skin electronics. *Smart Materials and Structures*, 20(10):105017, 2011.

[55] Yi Chen, Jillian M Oliveira, and Ian W Hunter. Two-axis bend sensor design, kinematics and control for a continuum robotic endoscope. In *IEEE International Conference on Robotics and Automation (ICRA)*, pages 704–710, 2013.

[56] Andreas Frutiger, Joseph T Muth, Daniel M Vogt, YiÇğit Mengüç, Alexandre Campo, Alexander D Valentine, Conor J Walsh, and Jennifer A Lewis. Capacitive soft strain sensors via multicore–shell fiber printing. *Advanced Materials*, 27(15):2440–2446, 2015.

[57] Helge A Wurdemann, Sina Sareh, Ali Shafti, Yohan Noh, Angela Faragasso, Damith S Chathuranga, Hongbin Liu, Shinichi Hirai, and Kaspar Althoefer. Embedded electro-conductive yarn for shape sensing of soft robotic manipulators. In *37th Annual International Conference of the IEEE Engineering in Medicine and Biology Society (EMBC)*, pages 8026–8029, 2015.

[58] Ali Abbas and Jianguo Zhao. A physics based model for twisted and coiled actuator. In *Robotics and Automation (ICRA), 2017 IEEE International Conference on*, pages 6121–6126. IEEE, 2017.

[59] SmoothOn. EcoFlex 00-10 Stifness url(https://www.smooth-on.com/products/ecoflex-00-10/).

[60] SmoothOn. EcoFlex 00-30 Stifness url (https://www.smooth-on.com/products/ecoflex-00-30/).

[61] Fei Jiang, Haijie Zhang, and Jianguo Zhao. Kinematics and statics for soft continuum manipulators with heterogeneous soft materials. In *ASME 2016 Dynamic Systems and Control Conference*, pages V002T25A004–V002T25A004. American Society of Mechanical Engineers, 2016.